GEOLOGICAL SURVEY OF CANADA
OPEN FILE 7763

Analysis of Measured Wind Turbine Seismic Noise Generated from the Summerside Wind Farm, Prince Edward Island

W.N. Edwards

2015

Canada

GEOLOGICAL SURVEY OF CANADA
OPEN FILE 7763

Analysis of Measured Wind Turbine Seismic Noise Generated from the Summerside Wind Farm, Prince Edward Island

W.N. Edwards

2015

1. Project Background

In the autumn of 2012, Health Canada (HC) proposed a one year duration scientific study to explore possible adverse health impacts to Canadians due to exposure to wind turbine generated noise. During the public consultation phase of the experiment, Natural Resources Canada (NRCan) approached Health Canada about its mutual interest in monitoring the environmental noise produced by modern wind turbine energy generation facilities or wind farms for the purposes of protecting current seismological and acoustic monitoring facilities in Canada. In the interests of cooperation and the success of the proposed project and having past experience in low frequency sound (or infrasound) monitoring technology, NRCan offered to assist HC in acquiring raw in-situ measurements of wind turbine noise. HC was receptive to the proposal and over the course of the next several months, details of the cooperative venture were discussed and planned. This planning culminated in the signing of an Interdepartmental Letter of Agreement or ILOA (Government of Canada, 2013).

In brief, the ILOA states that NRCan would supply a total of four remote stations capable of autonomous power and near real-time data acquisition, with each station containing a microbarometer and a seismometer to measure low-frequency sound and ground motion respectively within the frequency range of approximately 0.1 – 100 Hz. In addition to this equipment, a remote weather station would also be supplied by NRCan to continuously monitor the local meteorological conditions at 2 and 10 metres altitude, with all infrasound and meteorological data provided on a routine basis to HC. NRCan would also provide in-kind technical support to ensure the continuous operation and data collection of these stations over the course of the project.

At the end of 2012 it was mutually decided that the facility of study would be the Summerside Wind Farm, located to the north of the City of Summerside, Prince Edward Island. The facility consists of four (4) Vestas 3.0MW V-90 wind turbines and is owned and operated by the City of Summerside, with which HC arranged cooperation. The region to the east of the turbine facility was chosen as the most appropriate area for deployment of the seismo-acoustic stations as the area presented a relatively flat terrain and therefore was easily accessible and navigable for equipment installation and maintenance.

The period of active monitoring and deployment of the seismo-acoustic stations lasted for a period of approximately one year, operating from May 5, 2013 to May 22, 2014. The following report describes the preliminary analysis of the seismic observations of the Vestas V-90 wind turbines at the Summerside Wind Farm during this period.

2. Experimental Setup and Station Installation

The experimental area chosen during a meeting between HC, NRCan and MG Acoustics (a HC sub-contractor performing analysis on the collected infrasound data) was held early in 2013 to decide the appropriate locations for the monitoring stations. Four sets of properties were identified as prime locations for instrumentation to be located at approximate distances of 125 m, 2.5 km, 5.0 km and 10.0 km from the base of turbine #2 (Fig 1). These properties lay along a roughly east-southeast direction from the facility under study. Final locations of the equipment were determined after discussions with the appropriate land owners and coordinates of the four monitoring stations are provided in Table 1 (and shown in Fig 1), along with those of the four

Vestas V-90 wind turbines.

Station	Latitude (°N)	Longitude (°E)	Elevation (km)	Orientation (° E from N)
HC1P	46.43398	-63.79528	0.001	272
HC2P	46.43234	-63.76418	0.020	274
HC3P	46.42403	-63.73947	0.007	284
HC4P	46.41061	-63.67046	0.016	285
MetStn	46.43238	-63.76406	0.020	----
Turbine #1	46.43430	-63.80351	0.006	----
Turbine #2	46.43402	-63.79697	0.008	----
Turbine #3	46.44073	-63.79607	0.001	----
Turbine #4	46.43511	-63.80018	0.006	----

Table 1: Final locations of the installation of the seismo-acoustic monitoring stations, meteorological station and positions of the Summerside Vestas 3.0MW V-90 wind turbines (AMEC Earth & Environmental, 2009).

2.1 Seismo-Acoustic Monitoring Station Equipment

Each seismo-acoustic monitoring station was identical in design and components to allow both ease of installation and ongoing maintenance. Designed to be robust, weather resistant, autonomous and remotely accessible, each station was capable of independent uninterrupted power using a series of lead-acid batteries and solar recharging, along with cellular communication with the *EarthquakesCanada* datacenter in Ottawa. The following is a listing of the components that made up each station.

Infrastructure:
One (1) approximately 1.5m long High Density Polyethylene (HDPE) pipe with closed end cap
One (1) portable aluminum electronics case with fixed solar panel mounting brackets
One (1) flexible spatial filter consisting of four (4) 15 metre porous soaker garden hoses

Instrumentation & Acquisition:
One (1) Nanometrics Trillium 120PA broadband seismometer
One (1) Chaparral Physics Model-25 microbarometer
One (1) Nanometrics Trident 24-bit Digitizer
One (1) Global Positioning System (GPS) antenna
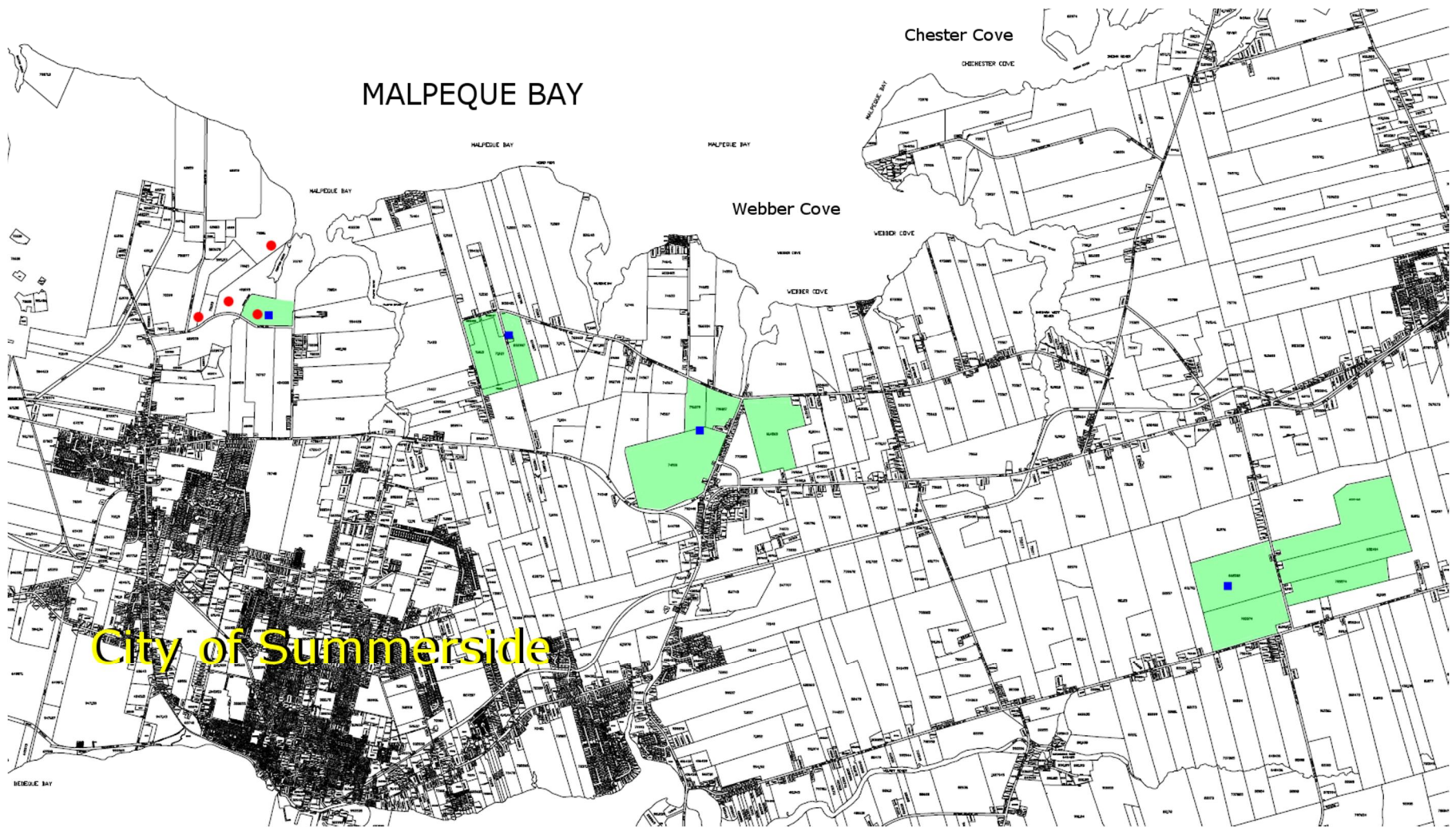
Remote Communications:
One Cellular VPN Modem
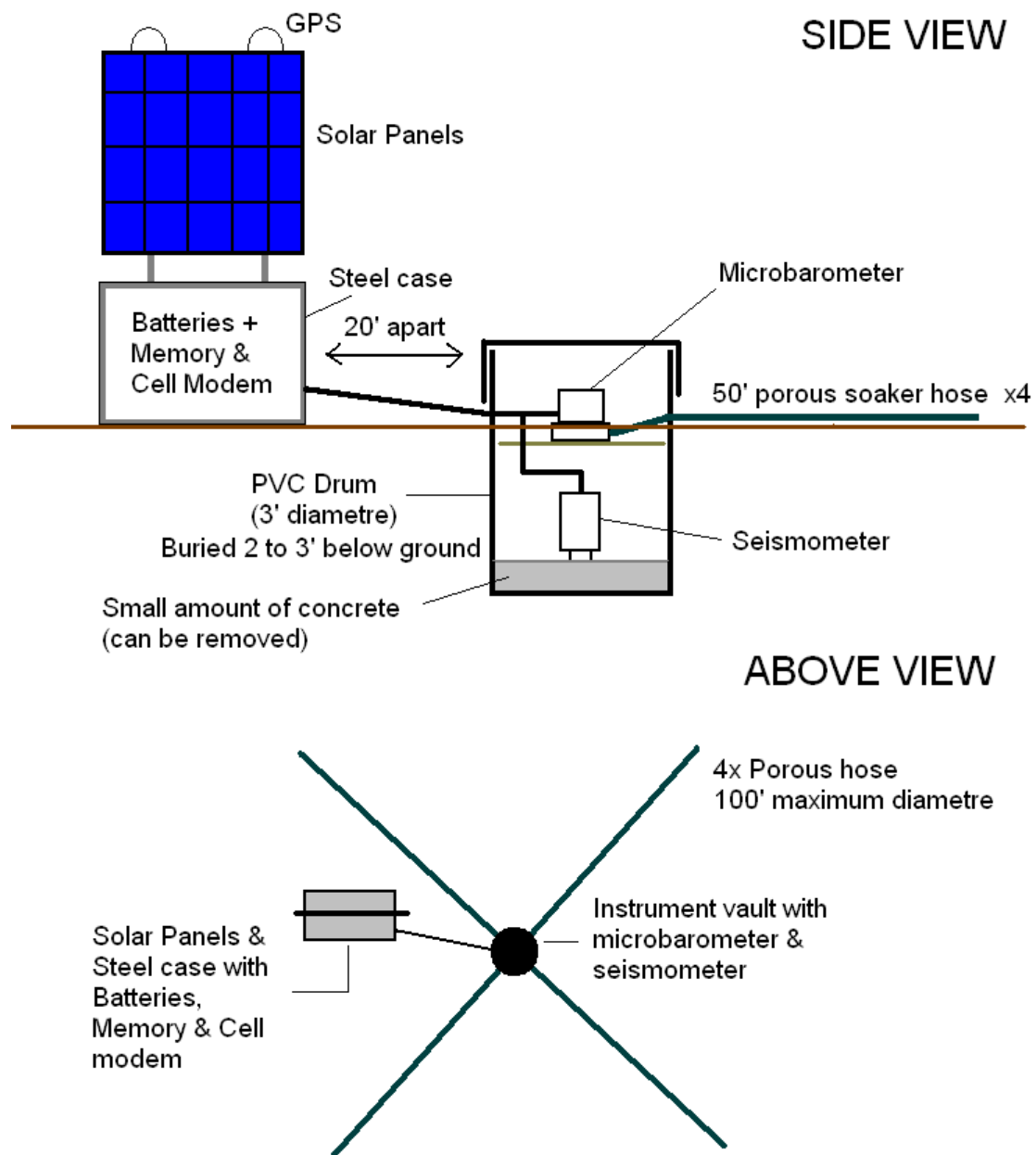
Remote Power:
Two (2) Kyocera 135 Watt solar panels
One (1) Sunsaver MPPT charge controller
Four (4) 12 Volt deep-cycle batteries

Configuration of the station is shown schematically in Fig. 2. With a minimum of equipment and infrastructure, stations operated autonomously with minimal maintenance over the yearlong deployment cycle, and easily removed during the recovery and remediation phase of the project.

Fig. 1: Land and property boundaries map for the region to the north and east of the City of Summerside, PEI. Potential proposed properties of interest for the installation of seismo-acoustic monitoring stations for this study are shown in green. Locations of the four Vestas 3.0MW V-90 wind turbines (red dots) lie to the north of the city. Optimal desired locations for stations lie at 125 m, 2.5 km, 5 km and 10 km from turbines. Final station locations are indicated by blue squares.

SIDE VIEW

GPS

Solar Panels

Microbarometer

Steel case

20' apart

Batteries +
Memory &
Cell Modem

50' porous soaker hose x4

PVC Drum
(3' diametre)
Buried 2 to 3' below ground

Seismometer

Small amount of concrete
(can be removed)

ABOVE VIEW

4x Porous hose
100' maximum diametre

Solar Panels &
Steel case with
Batteries,
Memory & Cell
modem

Instrument vault with
microbarometer &
seismometer

Fig. 2: Typical seismo-acoustic monitoring station setup. Station is designed to simultaneously record both seismic vibrations and infrasonic noise between frequencies of 0.1 – 100 Hz.

The monitoring instruments for these stations were chosen to provide a nominally flat response between 0.1 to 100 Hz, where both infrasonic and ground motion noise generated by wind turbines reside. Table 2 reports the instrument responses for the microbarometer and the seismometer in terms of mathematical poles and zeroes, while the shape of the response is shown in Fig. 3. Data sampling and system sensitivity rates were selected to assure adequate measurement of both relative pressure and ground motion without fear of clipping or saturation (off-scale measurements) over the course of the monitoring period. Sensitivity calibrations for both instruments are also provided in Table 2.

Instrument	Chaparral M25 Microbarometer	Nanometrics Trillium 120PA Seismometer
Poles (radians)	-1190	-0.03852 + 0.03658i
	-0.157 + 3.00x10⁻⁶i	-0.03852 – 0.03658i
	-0.157 – 3.00x10⁻⁶i	-178
	-0.157	-135 + 160i
	----	-135 – 160i
	----	-671 + 1154i
	----	-671 – 1154i
Zeroes (radians)	0	0
	0	0
	0	-90
	-4080	-160.7
	----	-3108
Normalization Factor (A0)	0.2917	308399
Normalization Period	1.0 second	1.0 second
Digitization Gain	1,000,000 Counts/V	1,000,000 Counts/V
Instrument Sensitivity	0.400 V/Pa	1200 V/(m/s)
Overall Sensitivity	400,000 Counts/Pa	1,200,000,000 Counts/(m/s)

Table 2: Instrument settings and sensitivities for the four seismo-acoustic monitoring stations

With these two instruments and a single three-channel digitizer at each station, only two of the three available channels (north-south, east-west, vertical) for seismic data were possible to record (the remaining channel on the digitizer being taken by the microbarometer's differential pressure data). Therefore each seismometer was rotated to align the north-south channel to an orientation that pointed radially towards Turbine #2 and the orientation noted (Table 1). The three recorded channels were then designated as HHZ (vertical seismic), HH1 (radial seismic) and HDF (infrasonic pressure) according to standard international seismological practice (Federation of Digital Seismographic Networks, 2012). Station names follow a common structure, "HC" associates the stations immediately with the Health Canada led project, numerals 1 – 4 were assigned based on increasing distance from the turbines for quick reference and the letter "P" would indicate the stations' location on Prince Edward Island, in accordance with standard Canadian National Seismic Network (CNSN) practice.

Fig. 3: Instrumentation of the seismo-acoustics stations. (Top Left) Model-25 microbarometer (manufactured by Chaparral Physics) measures minuscule variations in atmospheric pressure at infrasonic (below the threshold of human hearing) frequencies. (Top Right) Trillium Seismometer (manufactured by Nanometrics) measures minuscule vibrations in the ground. Primarily used to monitor and record earthquakes, the monitoring band of the Trillium seismometer overlaps that of the microbarometer for ease of data comparison. (Bottom) Bandwidth of the Model-25 and Trillium instruments in comparison to standard ISO/ANSI acoustic filter weightings. Both instruments are primarily sensitive to low acoustic and infrasonic frequencies.

2.2 Station Descriptions

HC1P

Located in the middle of a rural field immediately east of Turbine #2, specifically in the northwest field at the intersection of Lyle and Dekker Roads, this station is the closest of all four stations to the wind power generating facility. Its nominal distance of 125m from the base of Turbine #2 is dictated by the HC measurement requirements of having one point of observation at a standard distance of the tower's height (80 m) plus one blade length (45 m). Ownership of the land at the beginning of the study and time of installation was believed to be that of the City of Summerside, however, on September 25, 2013 the Project was informed that the station was instead on another private owner's property. After discussion with the landowner, HC was able to negotiate the station's continued presence at the site until the end of the study period (April 2014), under the stipulation that it would be the first station to be removed in order to allow the landowner to prepare the field for crops in the spring. The station is sheltered to the north by the wooded wetland area that surrounds much of the turbine facility property.

Fig 4a: Seismo-acoustic monitoring station HC1P as viewed to the west towards turbines #1 (hidden behind #2), 2, 4.

Fig 4b: Seismo-acoustic monitoring station HC1P as viewed to the north towards Turbine #3. In this view to the north, the treed wetland area can be seen in the distance, partially sheltering the station from winds from this direction.

HC2P

The second monitoring station is located ~2.5 km from the base of Turbine #2 at the site of a former farm house (now removed) on the side of a farm field along Waite Road, between Barbara Weit Road to the north and Sherbrooke Road to the south. Along with the monitoring station, the site also hosts the remote meteorological station (discussed in the next section). The station is generally open to the wind on all sides. Only a few unimposing trees immediately to the south bordering the former farm house property are near the station.

Fig. 5: Monitoring station HC2P after installation viewed looking to the southwest (above) and east (below). Note that in addition to the infrasonic and seismic monitoring instruments, the site also hosts the meteorological tower and equipment. Also note the few trees located to the south of the station, but otherwise the site is an open field.

HC3P

The third monitoring station is located ~4.5 km from the base of Turbine #2, similarly at the edge of a farmer's field. Located to the west of the access road (Rayner Creek Road) and further from it than HC2P, the station is sheltered from winds from the north by a small copse of trees, and from the southwest by a larger wooded area. These trees assist in reducing infrasonic noise caused by strong winds from those directions, but also increase the seismic background noise due to swaying transferring to ground motion through their roots.

Fig. 6: Monitoring station HC3P viewed from the south. In this view, the small copse of trees to the immediate north of the station can be seen providing the station some shelter from winds from that direction.

HC4P

The fourth and final monitoring station is located ~10 km from the base of Turbine #2 and was intended to provide a relative baseline measurement of conditions far from the wind turbine facility. Similarly situated on the edge of a local farmer's field, the station is located on the northwest corner of the intersection of MacIntyre and Blue Shank Roads, far from the roadside. The station is sheltered primarily from the west by a large wooded lot.

Fig. 7: Seismo-acoustic monitoring station HC4P as viewed looking west. The station lies on the edge of an open rural field, sheltered from westerly winds by a large wooded property.

2.3 Installation of the Meteorological Station

As specified in the ILOA, in addition to the monitoring equipment, NRCan supplied two meteorological instruments to monitor the local weather conditions. It was advised to HC during the planning phase that to minimize unnecessary expenditures (in the form of additional remote communications, power and land agreements) that this meteorological station (MetStn) be collocated with one of the seismo-acoustic monitoring stations. During the site selection HC, MG Acoustics and NRCan mutually agreed that the most appropriate site would be HC2P (Fig. 5), located ~2.5 km from the base of Turbine #2.

The MetStn consisted of two "all-in-one" Vaisala WXT-520 meteorological weather instruments designed to continuously monitor air temperature, humidity, atmospheric pressure, wind speed and direction. Although these instruments were also capable of measuring precipitation, this feature was not implemented. The two sensors were located at standard measurement heights of 2m and 10m. The infrastructure for the meteorological station included:

Infrastructure & instruments:
One (1) 10 metre tall, aluminum frame tower, with associated guy wires
Two (2) Vaisala WXT-520 weather transmitters
Two (2) Avisaro RS232 Dataloggers

Installation of the meteorological station coincided with that of the monitoring station HC2P on May 23, 2013.

All meteorological data were locally recorded and time-stamped by the dataloggers onto Compact Flash memory and remotely accessed four times daily to collect the previous day's data for parsing, distribution and archiving. A total of 5 measurement channels were monitored; outside temperature, humidity, atmospheric pressure, wind speed and wind direction. Sample rates of these channels were set to a 60 second period (0.0167 Hz) for temperature/humidity/pressure and a 5 second period (0.2 Hz) for wind parameters. Internally within the Vaisala WXT-520, these measurements represent an average over the sampling period of measurements made at one second intervals or 1 Hz. In the case of wind speed and direction, additional information regarding distribution of these measurements were provided in the data stream, in the form of the maximum and minimum speeds and directions recorded over the sampling interval. Time codes associated with all measurements represent the time at which the Avisaro dataloggers received the measurements from their respective weather stations.

Meteorological data channels were archived under the station code HC2P and the channel codes shown in Table 3 using standard seismological channel naming conventions (Federation of Digital Seismographic Networks, 2012).

Measurement	Channel name	Sample Period
Outside Temperature (ºC)	UKO	60 seconds
Outside Humidity (%)	UIO	60 seconds
Atmospheric Pressure (hPa)	UDO	60 seconds
Wind Speed (m/s)	VWS	5 seconds
Wind Direction (º)	VWD	5 seconds

Table 3: MetStn meteorological data channel codes and sampling periods.
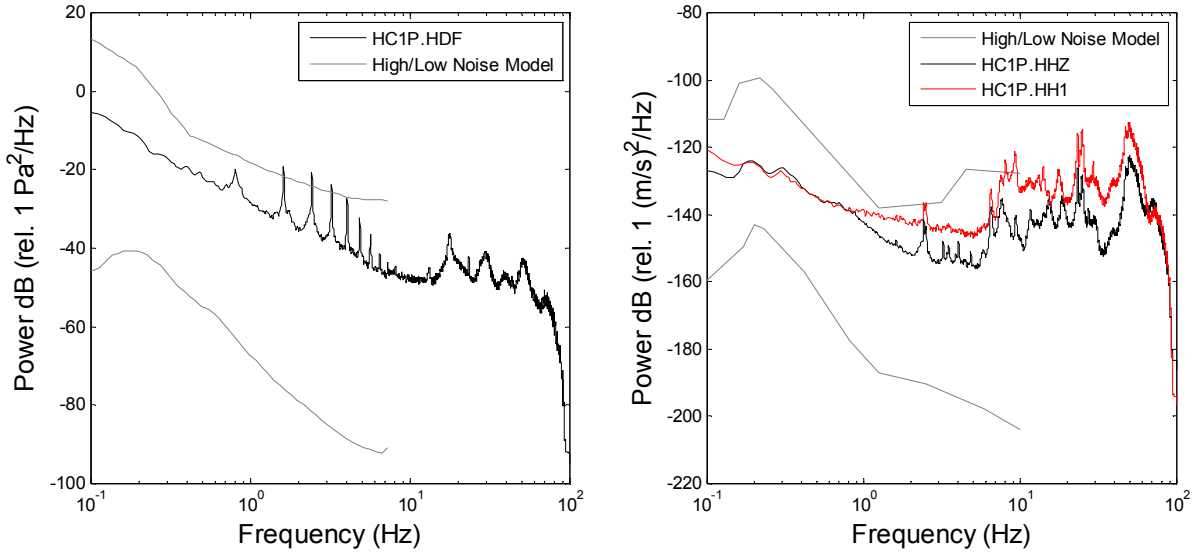
Fig. 8: Installation of the meteorological tower at the site of HC2P showing sensor observations at 2 and 10 metre heights.

2.4 Initial Data Evaluation
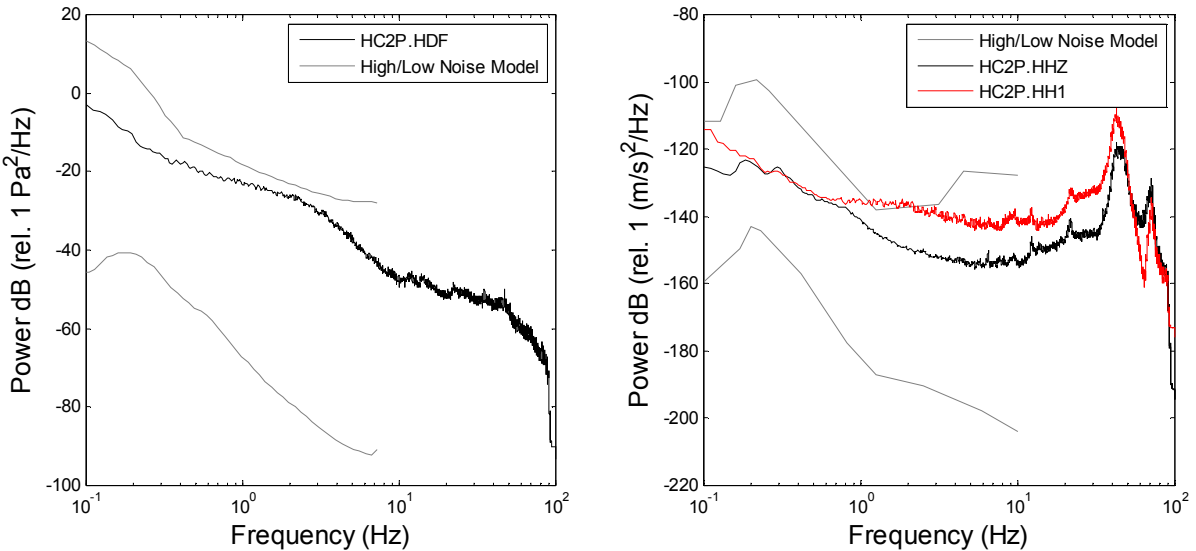
To evaluate the successfulness of the station installation a one hour segment of data was extracted from the real-time data stream and inspected on May 23rd, 2013 at 2000 UTC (5:00 pm ADT) at stations HC1P, HC2P, and HC3P and May 24th at 1900 UTC (4:00pm ADT) for station HC4P. Data showed no signs of clipping or artificial system induced noise. Spectral evaluation of the infrasonic channel (HDF) data showed that station noise levels fit within the upper quartile of the typical global ambient infrasonic noise background (Figs. 9-12, Bowman et al. 2005). As the Bowman et al. (2005) noise data are derived from international monitoring stations that often are located in remote regions, sheltered by dense tree/foliage cover and attached to significant noise reduction systems, it is not unexpected that the largely open air sites of this study, located in semi-rural settings and exposed to uninterrupted wind turbulence, close to urban noise sources would have noise spectra in the upper regions of the global noise spectrum. Of note within the observed spectrum of HC1P (Fig. 9) were several prominent spectral peaks at harmonic frequencies, likely associated with infrasonic waves produced by the nearby turbines. These frequencies appear to be limited to below ~20 Hz.

Inspection of seismic data from the same extracted hours similarly show no sign of clipping or loss of dynamic range indicating current settings are appropriate. Spectral evaluation of the seismic data segment also shows that typical station seismic noise is in the upper quartiles of the global ambient seismic noise distribution (Peterson 1993), with significant peaks throughout the higher frequencies of the frequency band of 0.1-100 Hz (Figs. 9-12). This was not unexpected due to the proximity of the stations to the turbines, and other sources of seismic noise such as urban/rural roadways and the stations' installation on local soil rather than bedrock.
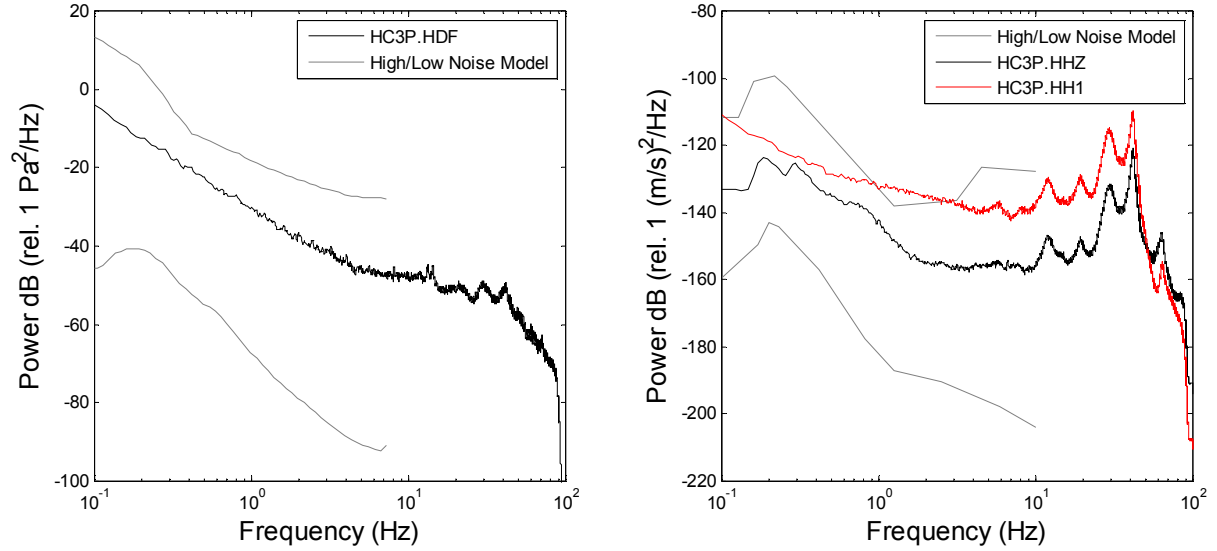
Conclusions after data inspection were that station installation went as planned and that acquisition settings of the digitizers were appropriate for successful recording of noise levels during the monitoring period.
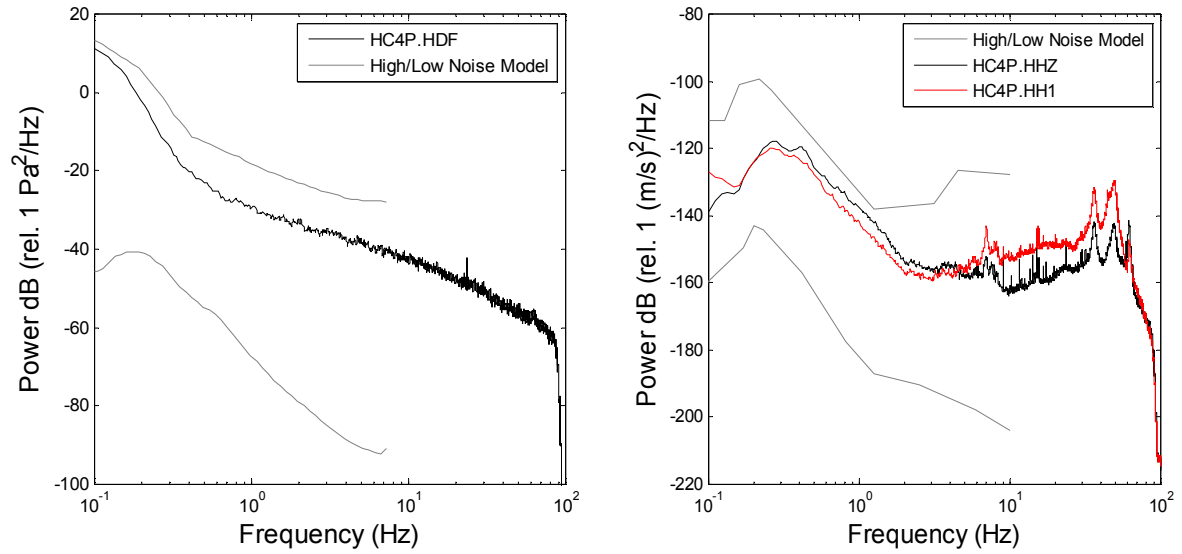

Fig. 9: Power spectral density of initial 30 minutes of data acquisition at station HC1P on May 23, 2013 at 2000 UTC. Infrasonic channel HDF (left); Seismic vertical channels (right) HHZ (black) and radial HH1 (red). Ambient high and low noise models of infrasound (Bowman et al. 2005) and seismic ground motion (Peterson 1993) are shown in grey.

Fig. 10: Power spectral density of initial 30 minutes of data acquisition at station HC2P on May 23, 2013 at 2000 UTC. Infrasonic channel HDF (left); Seismic vertical channels (right) HHZ (black) and radial HH1 (red). Ambient high and low noise models of infrasound (Bowman et al. 2005) and seismic ground motion (Peterson 1993) are shown in grey.

16

Fig. 11: Power spectral density of initial 30 minutes of data acquisition at station HC3P on May 23, 2013 at 2000 UTC. Infrasonic channel HDF (left); Seismic vertical channels (right) HHZ (black) and radial HH1 (red). Ambient high and low noise models of infrasound (Bowman et al. 2005) and seismic ground motion (Peterson 1993) are shown in grey.


Fig. 12: Power spectral density of initial 30 minutes of data acquisition at station HC4P on May 23, 2013 at 2000 UTC. Infrasonic channel HDF (left); Seismic vertical channels (right) HHZ (black) and radial HH1 (red). Ambient high and low noise models of infrasound (Bowman et al. 2005) and seismic ground motion (Peterson 1993) are shown in grey.

17

3. Data Processing: Meteorological and Spectral

Analysis of the general noise characteristics and properties of the Vestas 3.0MW V-90 wind turbines at the Summerside Wind Farm requires a robust measure of the most common noise performance observed during the monitoring period. Rather than isolating the noise performance of the turbines at any one specific point in time, data that statistically share common characteristics were grouped, stacked and statistically averaged. The common characteristic that was used was wind speed, which should correlate with a common power output by the turbines.

Although meteorological data from the study is available at both near-ground level (2 m) and at 10 m heights, it is most useful to have the wind speeds measured at the elevation of the turbine nacelle, or 80 m, where it powers the turbine blades. While meteorological information is typically gathered by the facility operators as an operational requirement, this data was not made generally available for study at the time of analysis. To fill this information gap, the wind speeds measured at the 10 m elevation were used to extrapolate to those at 80 m using a standard wind shear power law (Panofsky and Dutton, 1984).

$$U = U_{ref}\,(\,Z\,/\,Z_{ref}\,)^{\alpha} \tag{1}$$

where U is the wind speed at the desired height (80 m), U_{ref} is the measured wind speed at a known height (10 m), Z/Z_{ref} is the ratio of the desired and reference heights and α is the Hellman or wind shear exponent. For the purposes of the remainder of the analysis, the value of the shear exponent was taken as 0.22. This particular value is used to be consistent with the modelled mean wind speeds provided by the Canadian Wind Energy Atlas (Environment Canada, 2008, http://www.windatlas.ca/en/links.php) for the study region and is typical for areas of rural crops with few or short trees.

After extrapolation of the 10 m height wind speed data to a turbine nacelle height of 80 m, the individual wind speed measurements were averaged over a 10 minute period over the course of the monitoring year and used to define a specific time period for spectral computation. For each 10 minute segment, the power spectral density (PSD) of the infrasonic (HDF) and vertical seismic (HHZ) data were computed using the method of Welch (1967) with a one minute long Hanning window and a 50% overlap. All computed PSD spectra for the two channels were then sorted into wind speed groups with 1 m/s increments from 1 m/s to 20 m/s, encompassing the majority of wind speeds encountered during the monitoring period and operational specifications of the V-90 turbines (Vestas, 2006).

With the computation of many PSD spectra from time segments under similar wind conditions, the spectra are stacked and averaged to substantially reduce the amount of variance in spectral information observed in any singular spectrum. Localized turbulence, changes in ambient conditions (such as humidity, temperature, large scale weather), or transient sources (such as vehicular traffic, earthquakes, severe storms etc.) can all contribute to increased spectral variance in any individual PSD spectrum. Thus by grouping and then averaging over a large number of common spectra, a significantly smoother and robust spectrum can be achieved with a variance reduction that approaches a factor $1/\sqrt{N}$.

After grouping the various spectra falling within a common wind speed, the spectral distribution

was computed at each frequency and the upper 75th and lower 25th percentiles were removed prior to computation of a mean or average. As infrasonic and seismic spectral power may vary over several orders of magnitude and as such are often represented on logarithmic scales, the removal of the upper and lower 25th percentiles helps to ensure that any mean spectrum is not adversely affected by extreme spectral outliers, making the final inner-quartile mean a more robust measure of the average spectrum during each wind condition than the explicit mean of all spectra. This process was repeated for each wind speed category. For the following analysis, the number of spectra used to compute each inner-quartile mean is given in Table 4.

All measurements in the following analysis are then taken in reference to the inner-quartile mean spectrum for a specific wind speed category. Use of the upper 75th and lower 25th percentile spectra are used to provide upper and lower limits on these measurements respectively.

Wind Speed	HC1P HDF	HC1P HHZ	HC2P HDF	HC2P HHZ	HC3P HDF	HC3P HHZ	HC4P HDF	HC4P HHZ
0 – 1 m/s	326	325	321	331	324	325	316	330
1 – 2 m/s	1697	1706	1643	1695	1658	1709	1626	1715
2 – 3 m/s	1994	1992	1926	1998	1919	2016	1894	2010
3 – 4 m/s	2479	2477	2390	2484	2362	2520	2329	2498
4 – 5 m/s	2405	2388	2365	2422	2351	2429	2297	2427
5 – 6 m/s	2225	2234	2197	2261	2201	2268	2185	2291
6 – 7 m/s	2354	2334	2296	2382	2307	2383	2307	2391
7 – 8 m/s	2353	2367	2296	2368	2308	2400	2268	2416
8 – 9 m/s	2268	2291	2216	2275	2195	2306	2183	2355
9 – 10 m/s	2035	2058	2004	2044	1972	2077	1987	2106
10 – 11 m/s	1818	1829	1793	1805	1750	1860	1780	1887
11 – 12 m/s	1685	1684	1659	1685	1647	1705	1642	1724
12 – 13 m/s	1413	1403	1402	1397	1369	1399	1374	1425
13 – 14 m/s	1196	1179	1186	1194	1161	1187	1151	1195
14 – 15 m/s	800	791	787	799	779	795	748	799
15 – 16 m/s	669	658	670	671	665	665	643	668
16 – 17 m/s	517	515	514	516	507	514	499	516
17 – 18 m/s	413	416	422	423	413	411	418	426
18 – 19 m/s	328	331	321	328	322	326	319	327
19 – 20 m/s	267	267	256	266	254	265	248	258

Table 4: Number of individual 10 minute data windows used to compute the inner-quartile mean for each wind speed category for each monitoring station and channel. Each 10 minute data window was segmented into nineteen, 1 minute windows overlapped by 50% and used to compute a power spectral estimate. These estimates were then averaged to obtain a mean spectrum with which to describe the 10 minute data window, following the procedure of Welch (1967).

3.1 Infrasound Observations of Noise
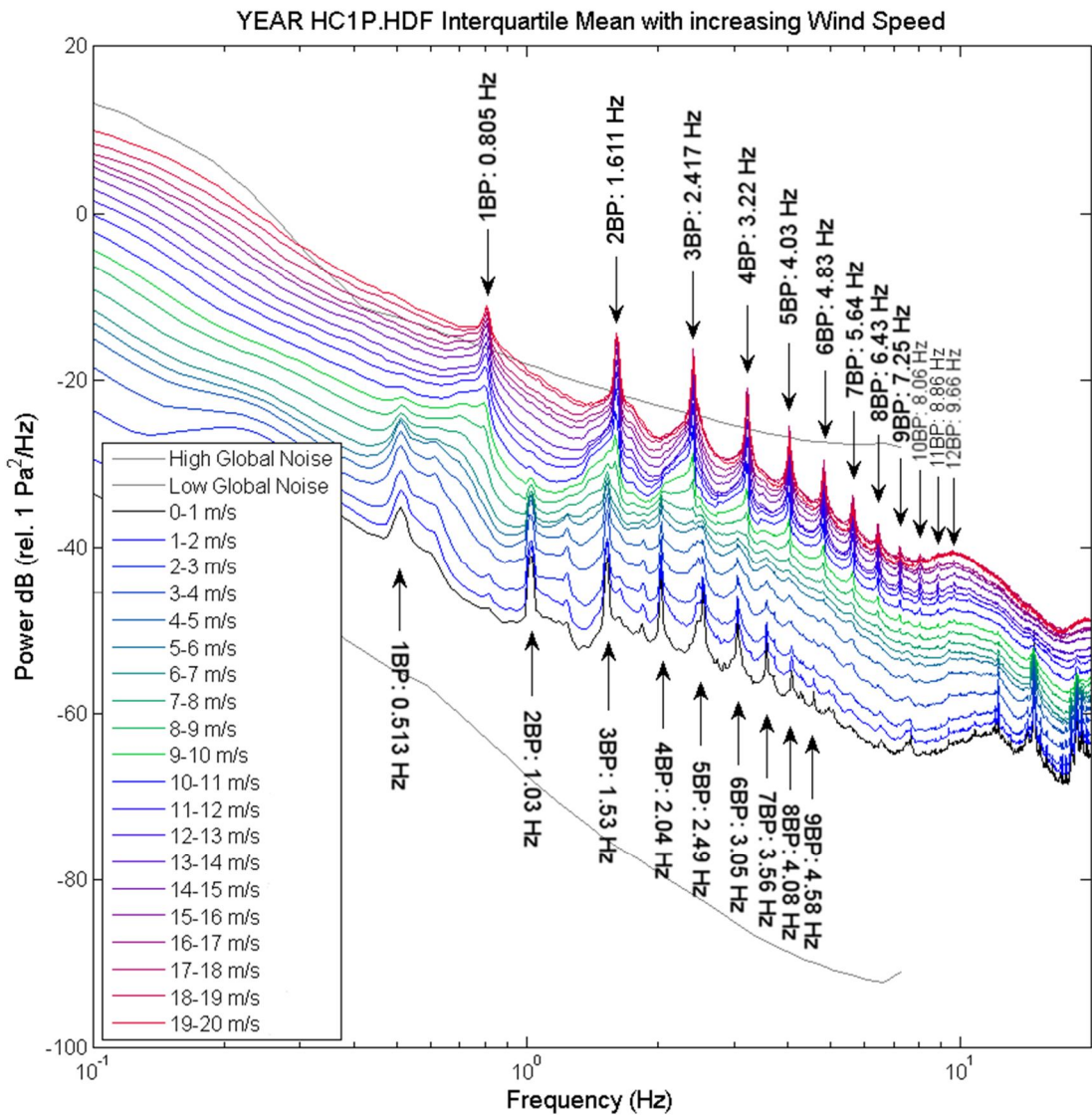
Using the methodology outlined in the previous section, the inner-quartile mean was calculated for winds ranging from calm conditions (winds < 1 m/s or 3.6 km/h) to a maximum of 20 m/s or 72 km/h for the four monitoring stations located approximately 0.125, 2.5, 5.0 and 10.0 km from the Summerside wind turbines. These mean spectra are shown in Figs. 13 – 16 alongside the high and low global infrasonic noise spectra of Bowman et al. (2005). In all cases, noise associated

with the operation of the wind turbines is limited to frequencies between 0.1 and ~10 Hz.
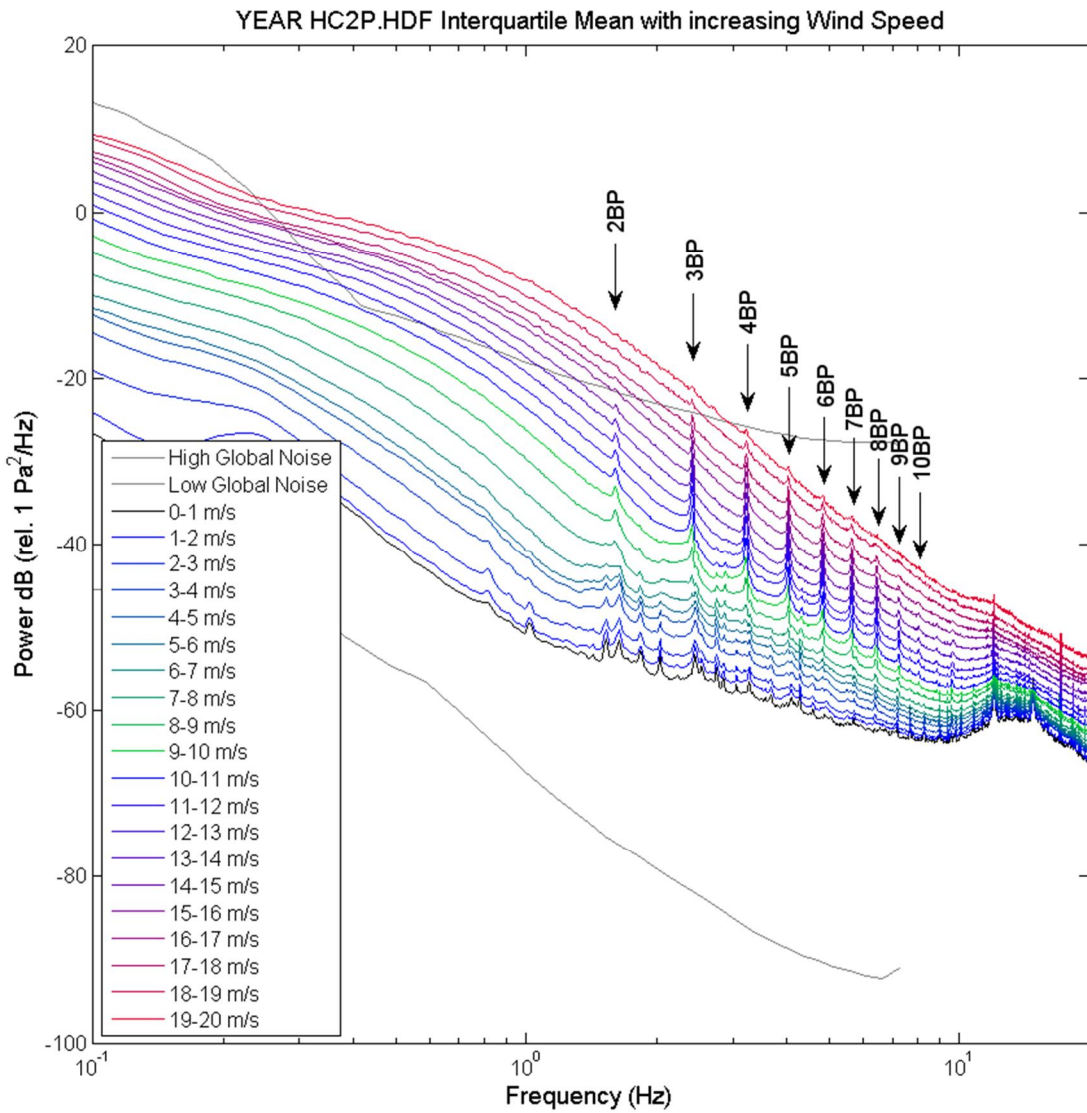
The character of the noise observed from the V-90 wind turbines within the infrasound band appears to be that associated with the rotation of the turbine blades and are comprised of several harmonic peaks associated with a fundamental frequency of 0.513 Hz at low wind speeds less than ~8 m/s, and transitioning quickly to 0.806 Hz at higher wind speeds (Fig. 13). These frequencies would correspond to rotation rates of the turbine blades of 10.3 and 16.1 RPM (rotations per minute), respectively, which correspond well to the nominal range of rotor rotation of 9.9 – 16.1 RPM provided in the Vestas V-90 specifications (Vestas, 2006).

The source mechanism for this type of observation has been previously established to be associated with the passage of the turbine blades in-front of the turbine tower (van den Berg, 2005, Moller and Pedersen, 2011). As the blades pass the tower, turbulent air is compressed between the blade and the tower creating an impulse. This impulse is repeated each time one of the three blades pass the tower. As these impulses are not continuous, the repeated action results in a modulation of the fundamental frequency alongside multiple of its higher harmonics (Fig 13). Propagating outward from the turbines, these infrasonic impulses can be seen on all four monitoring stations with decreasing amplitude and power (Figs. 13-16). As both the power of the ambient infrasonic background noise and the turbine blade-pass noise are functions of the wind speed, the ability to detect the turbines becomes a competition between the growth of the ambient background, the increase in turbine noise and the distance from which the measurement is made.
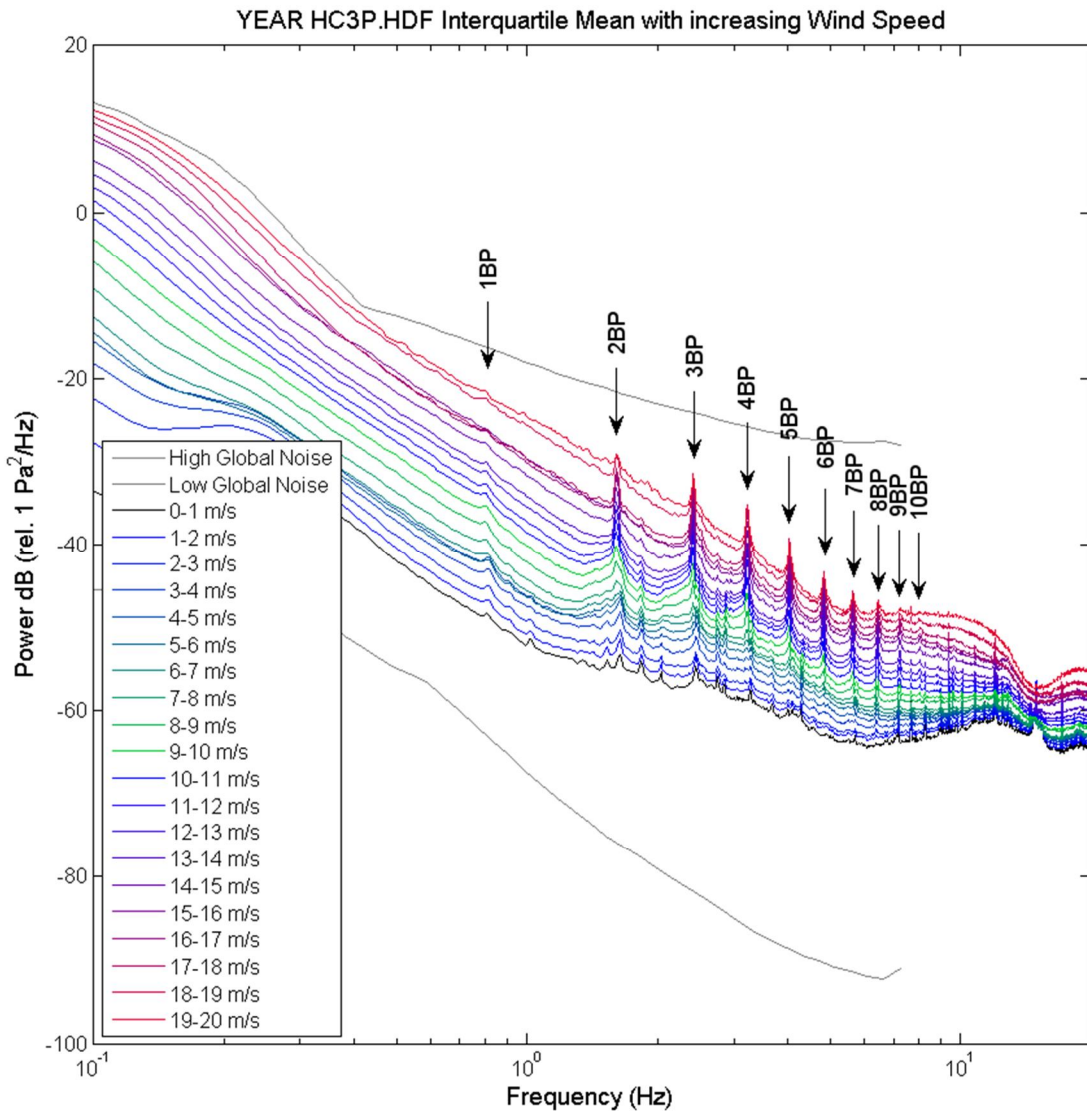
A complete analysis of the behavior of the infrasonic component of the turbine noise is beyond the scope of this specific report. It is however relevant in establishing the presence and source of this noise before discussion of similar noise structure observed in the seismic component of the monitoring study.
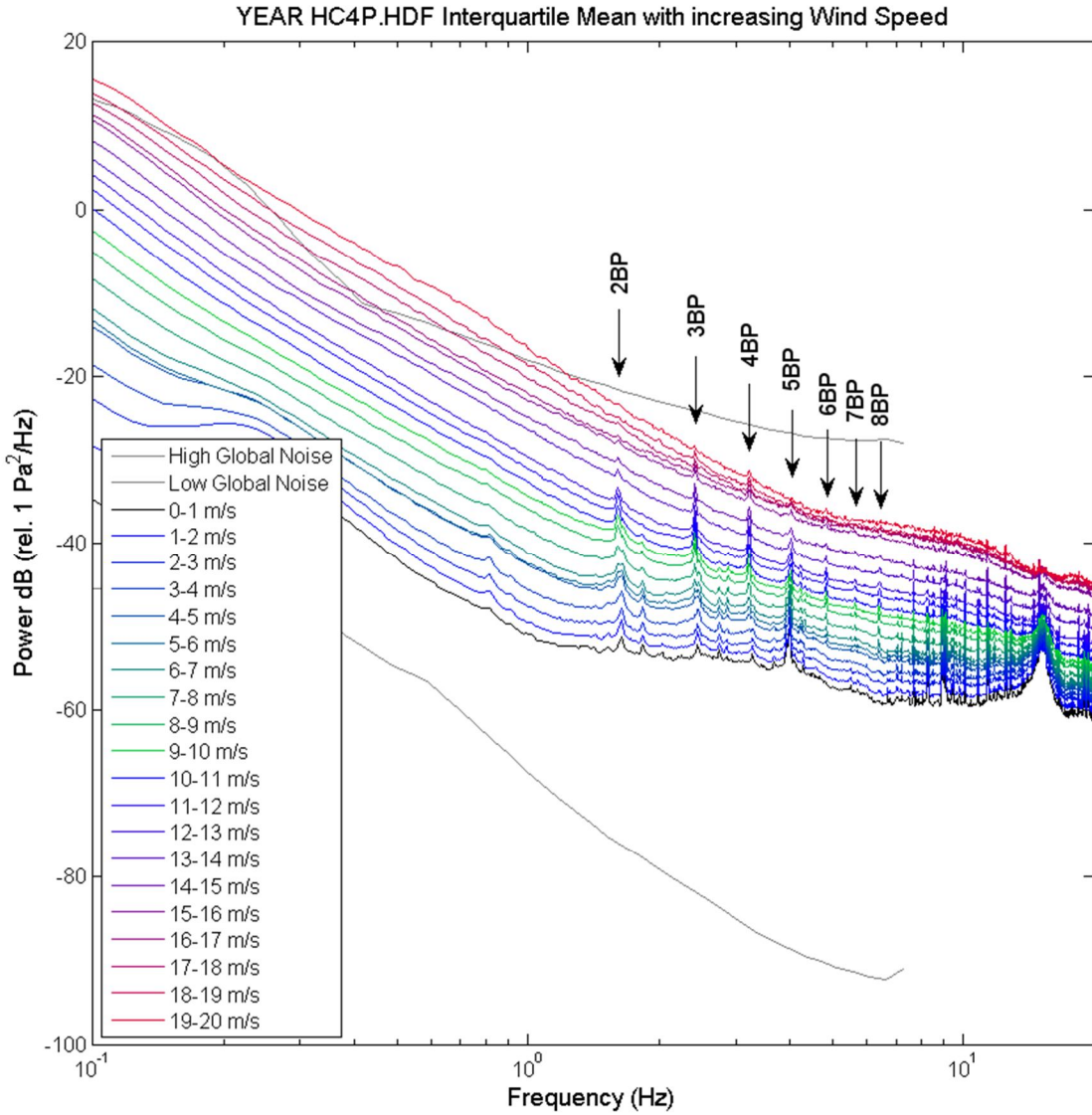
Fig. 13: Inner-quartile means for a range of wind speeds as observed infrasonically at monitoring station HC1P located ~125 m from the base of turbine #2. Observed noise source is primarily that of harmonics of the V-90 turbine blade-pass (BP) frequency, which is initially slow at low wind speeds and quickly increases to its peak 16.1 RPM value between winds of ~7 − 8 m/s.

Fig. 14: Inner-quartile means for a range of wind speeds as observed infrasonically at monitoring station HC2P located ~2.5 km from the base of turbine #2. Observed noise source is primarily that of the V-90 turbine blade-pass harmonics (BP). A more rapid increase in ambient background levels between 0.03 – 4 Hz result in a near-burial of the turbine harmonics at high wind speeds. This is likely due to the greater exposure of the HC2P site to wind turbulence as compared to the other three monitoring stations.

Fig. 15: Inner-quartile means for a range of wind speeds as observed infrasonically at monitoring station HC3P located ~5.0 km from the base of turbine #2. Observed noise source is primarily that of the V-90 turbine blade-pass harmonics (BP). A more gradual increase in ambient background levels allows the turbines blade-pass harmonics to be readily identifiable during high winds as compared to HC2P.

Fig. 16: Inner-quartile means for a range of wind speeds as observed infrasonically at monitoring station HC4P located ~10.0 km from the base of turbine #2. Observed noise sources are primarily a combination of the V-90 turbine blade-pass harmonics (BP) and local, likely anthropogenic, sources at frequencies greater than ~7 Hz.

3.2 Seismic Observations of Wind Turbine Noise
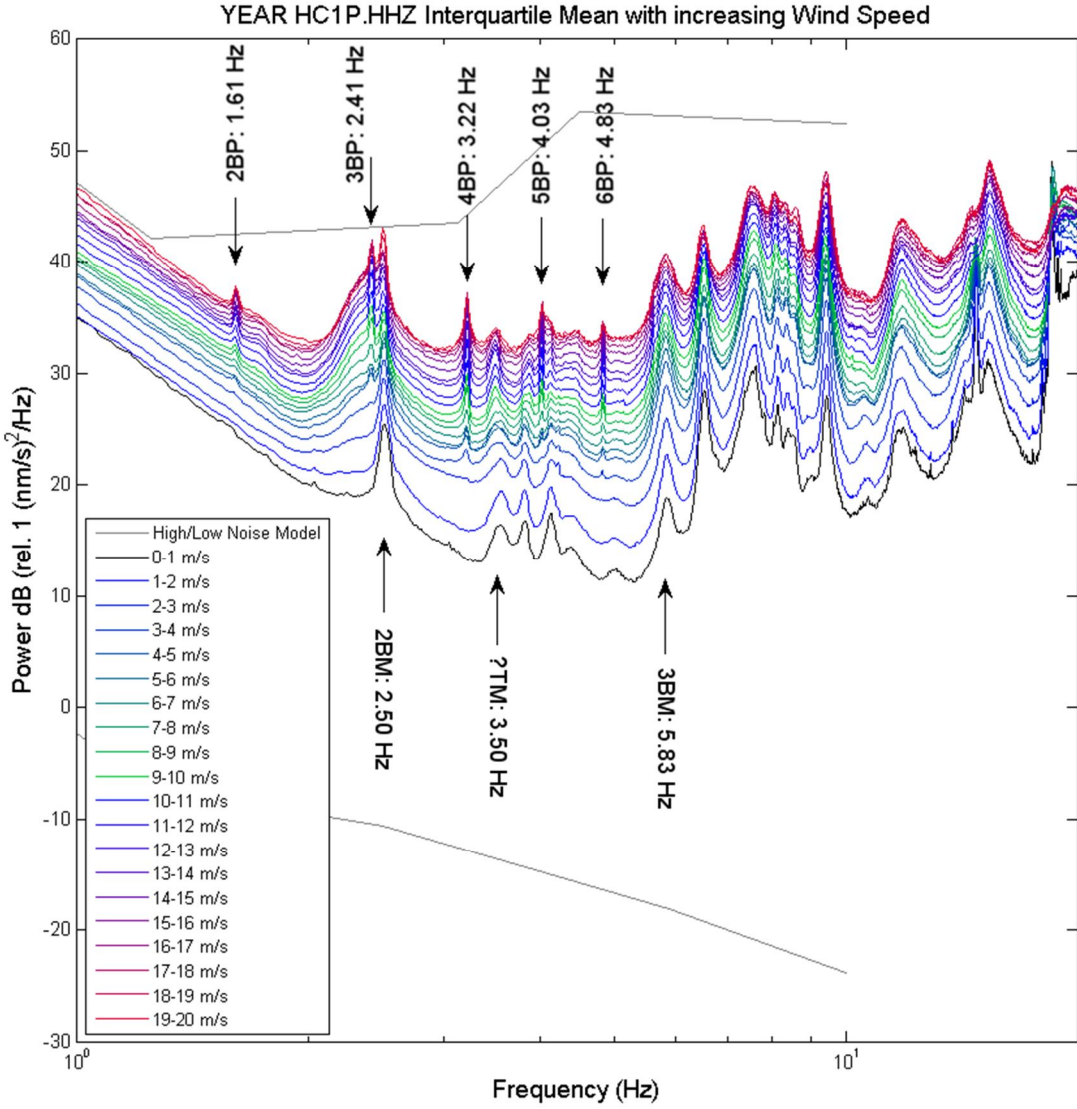
Similar to the infrasound observations discussed and shown in the preceding section, vibrations associated with the Summerside V-90 wind turbines and the turbine infrastructure are observed on all four of the seismo-acoustic monitoring stations. Sources of turbine vibration stem from similar mechanisms to that of infrasound, namely the turning of the turbine blades, with the additional complexity that any vibration of the turbine tower is transferred mechanically to the ground through the tower's foundation. Thus not only are the various harmonics of a turbine's blade-pass frequency observed as the compressed air pushes back on the tower, but also structural vibrations

24

be they flexural or torsional modes of the tower, are recorded. With modern wind turbine towers reaching nearly 100m heights, these structures act like inverted pendulums with fundamental modes ranging from several seconds period to a few Hertz (e.g. Nuta et al. 2011).
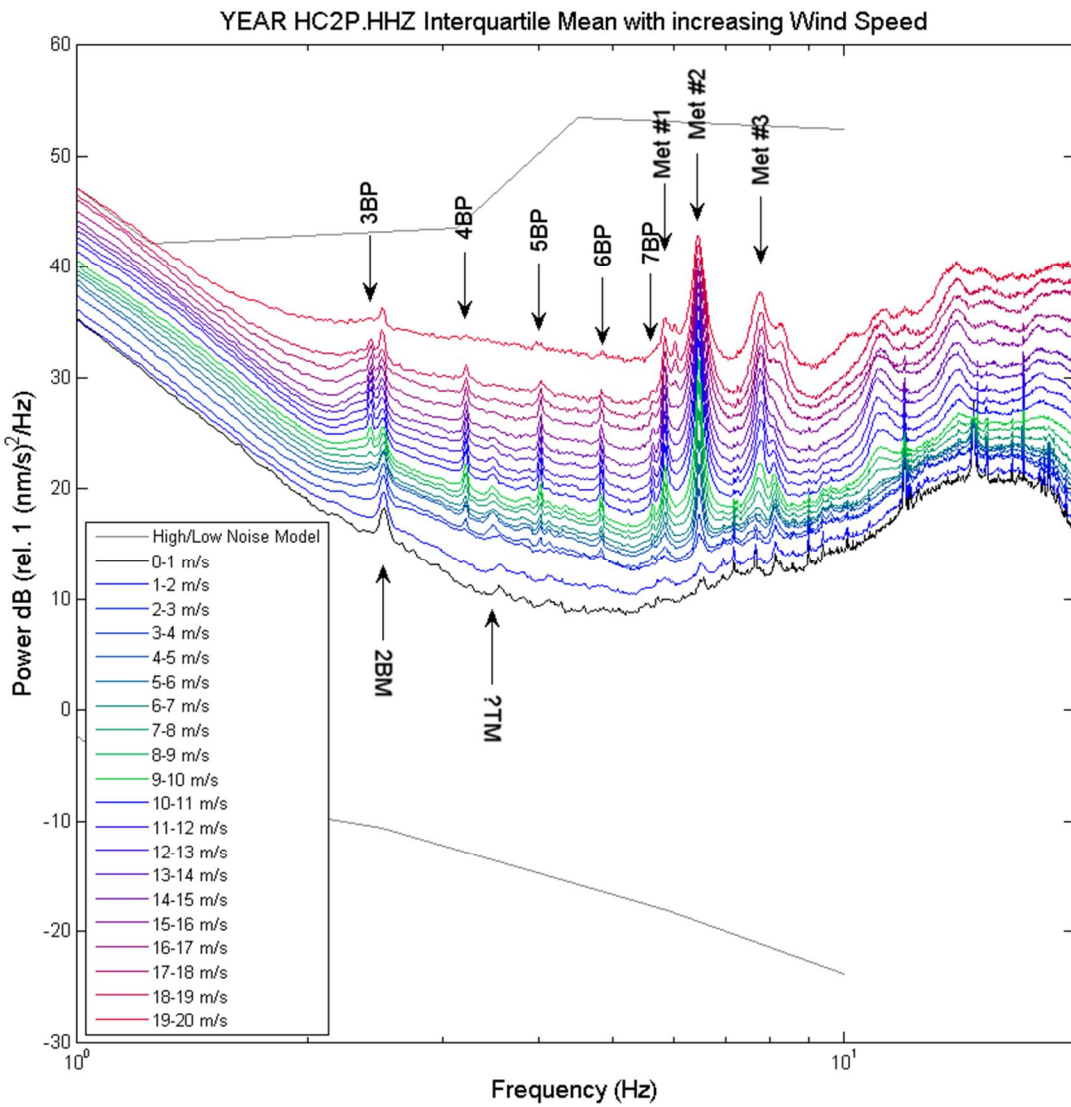
The numerous structural modes possible can be readily seen on monitoring station HC1P located only 125 m from the foundation of Summerside turbine #2 (Fig. 17). At this station, even during the calmest of wind conditions (black line, Fig. 17), where no blade-pass harmonics are visible and rotation of the turbine blades may be minimal, the number of broad spectral peaks that may be associated with structural modes of the turbine tower, exceed 15 at frequencies greater than ~1 Hz. This suggests that even without significant rotation of the turbine blades, sufficient force is exerted upon the tower to induce measureable vibrations. However, without detailed information and/or modelling of the possible modes of the V-90 tower, it is difficult to identify which peaks may be associated with any specific flexural or torsional mode, save possibly a few.

Investigating seismic response of wind turbine infrastructure during significant earthquakes, Nuta et al. (2011) used Finite Element Modelling (FEM) to predict the first three flexural or bending modes for a typical 80 metre tall tubular turbine tower for a 1.65 MW wind turbine at 3.17, 0.39 and 0.17 second periods, or 0.32, 2.56 and 5.88 Hz respectively. The prominent spectral peak observed on HC1P at 2.50 Hz is located at a similar frequency as that predicted for the second bending mode (2BM) of the 80m tower. As the Vestas V-90 towers are comparable in height (Vestas 2006), and have a similar tubular tower design (Figs. 4a/b) to the Nuta et al. model, an association of this peak with the second bending mode is not unreasonable. A similar peak is observed on HC1P at 5.83 Hz which may correspond to the third bending mode (3BM, Fig. 17). Extending this inference to the fundamental bending mode however becomes difficult as the predicted fundamental tower mode lies within the part of the spectrum occupied by the prominent microseism peak (an omnipresent band of seismic noise between ~0.15 and 0.5 Hz generated by seismically coupled wave interactions in the Earth's oceans) and so may be masked by the ambient background, making it difficult to identify. Finally a common minor peak is seen on both HC1P and HC2P at ~3.50 Hz or 0.28 seconds (Figs. 17, 18) at all wind speeds for HC1P and low to moderate wind speeds at HC2P before background noise buries the signal. While currently the mode to which this peak belongs remains unknown, based on the behavior of its spectral growth with wind speed (Section 4.0) compared to the 2BM and 3BM, the peak appears to be associated with the turbine tower and may represent either another bending mode or possibly a torsional mode (?TM). Unfortunately this association remains tentative as a complete finite element vibrational analysis of the turbine structure such as that of Nuta et al. (2011), which might uniquely identify this mode's source, is beyond the scope of this study.
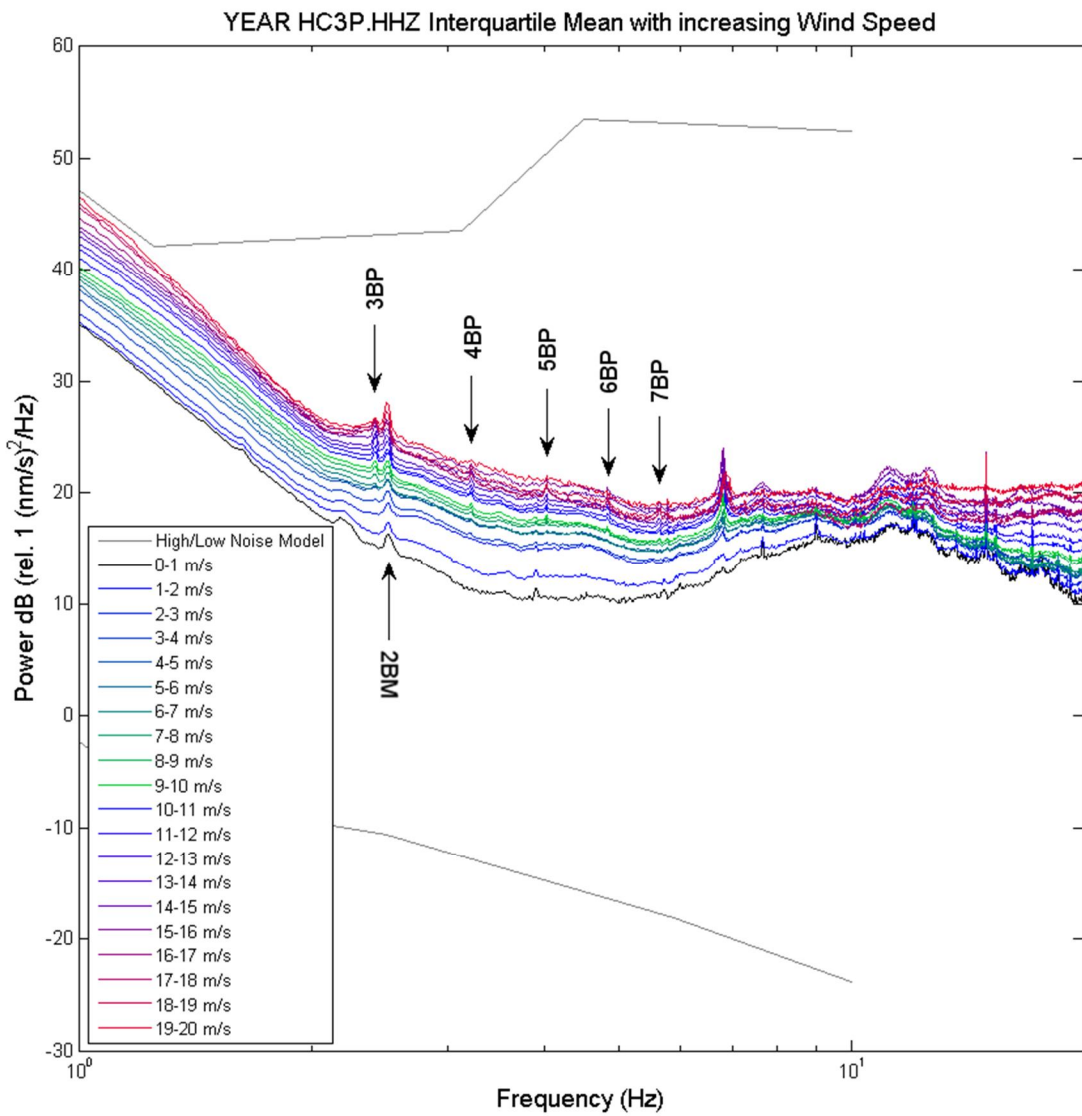
In addition to structural modes of the tower, peaks associated with the blade pass frequency of the turbine blades are also observed within the ground motion spectrum during higher wind speeds and can be observed at all monitoring stations (Figs. 17 – 20). At HC1P, five blade-pass harmonics ranging from the 2nd to the 6th can be identified before numerous prominent structural modes dominate the spectrum. In the far field, at ranges of 2.5 km and greater, most of the turbine tower modes are not observed beyond the 2BM and 3BM modes (Fig 18 – 20), suggesting that the near-field spectrum measured near the base of the tower at HC1P is not a suitable spectrum to use in order to predict the far field spectrum for the Vestas V-90 turbines. A similar conclusion was reached by Saccorotti et al. (2011) during monitoring of four 2.5 MW turbines close to the LIGO gravity wave observatory near Pisa, Italy.
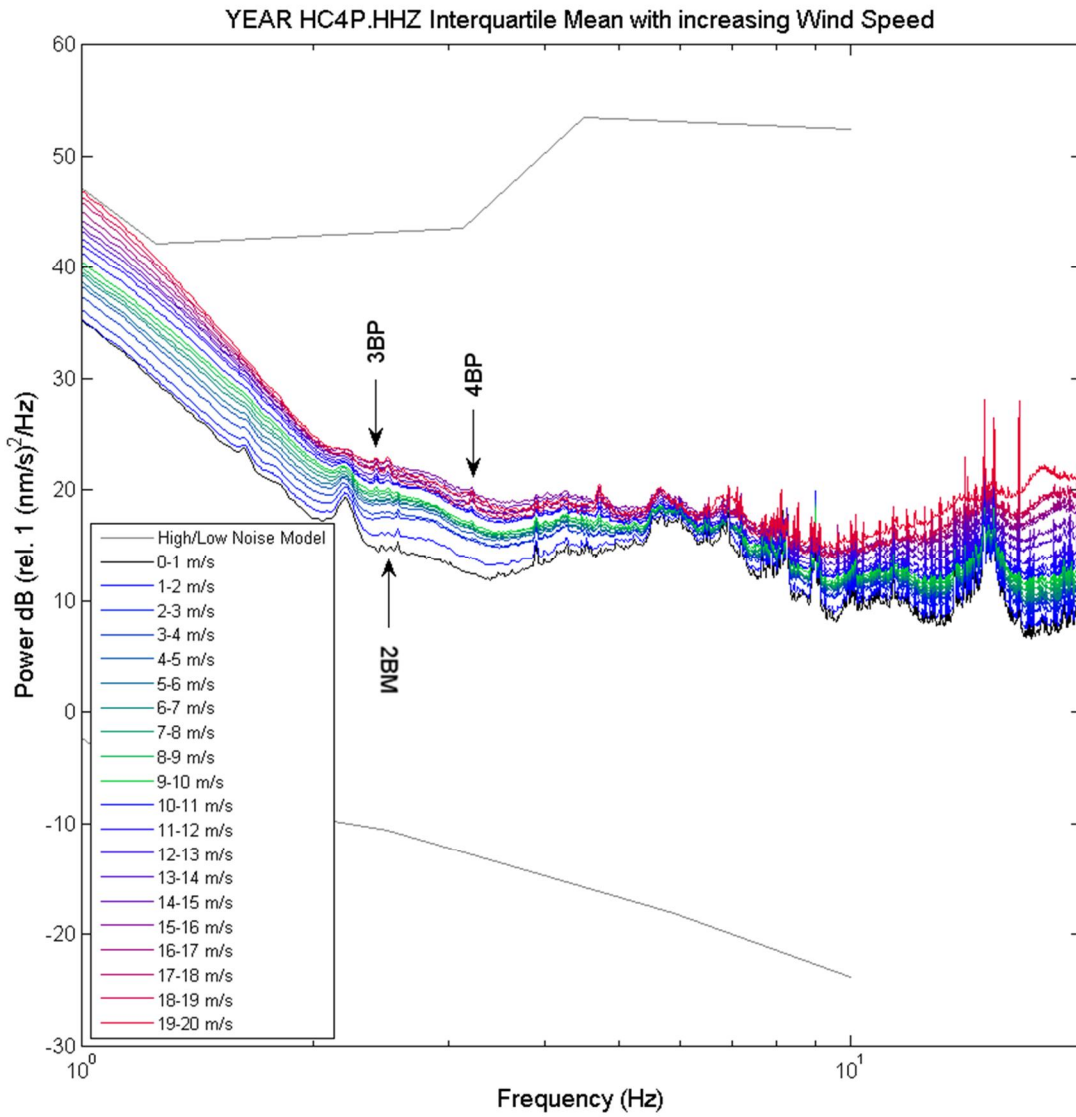
Fig. 17: Inner-quartile means for a range of wind speeds as observed seismically at monitoring station HC1P located ~125 m from the base of turbine #2. Observed noise shows a significant number of spectral peaks at frequencies > 1 Hz, many of which are likely due to structural flexural and torsional modes of the wind turbine tower, as well as several peaks that are associated with turbine blade-pass frequency harmonics (c.f. Fig 13). Identifiable structural modes, due to FEM modelling of a similar tower by Nuta et al. (2011), occur at 2.50 and 5.83 Hz and are likely associated with the second and third bending modes of the tower (2BM, 3BM).

Fig. 18: Inner-quartile means for a range of wind speeds as observed seismically at monitoring station HC2P located ~2.5 km from the base of turbine #2. Observed noise shows multiple harmonics of the turbine blade pass frequency (c.f. Fig 14), along with the tower's 2BM. Three additional strong peaks are seen at 5.85, 6.46 and 7.76 Hz and are likely associated with the sway and vibrations of the 10m tall meteorological tower (Met#1-3) which was collocated with HC2P (Fig. 5).

Fig. 19: Inner-quartile means for a range of wind speeds as observed seismically at monitoring station HC3P located ~5.0 km from the base of turbine #2. Observed noise shows primarily the turbine tower's 2BM, along with several harmonics of the blade pass frequency at higher wind speeds (c.f. Fig. 15).

Fig. 20: Inner-quartile means for increasing wind speeds as observed seismically at monitoring station HC3P located ~5.0 km from the base of turbine #2. Observed noise shows primarily ambient background sources likely of local anthropogenic origin, however, both the turbine tower's 2BM, and a few harmonics of the blade pass frequency can be identified at higher wind speeds.

4. Noise Measurements and Spectral growth

Measurements of spectral noise power associated with peaks described in the preceding section were measured at all four monitoring stations to observe their behavior, both at the source and at increasing distances from the Summerside turbines. Measurements were carried out by integrating the area beneath the inner quartile mean power-spectral-density function (Figs. 17-20) within a narrow band encompassing each specific peak (when observed), for each of the four seismo-acoustic monitoring stations. This procedure provides measure of the RMS power within the frequency band and is proportional to the square of the RMS ground motion amplitude with units

of velocity squared. Equivalent measurements were taken at both the 75th and 25th percentiles to provide upper and lower limits to the RMS ground motion, respectively. This measurement procedure was carried out at each wind speed and the results are summarized in Tables 5-8. In general, upper and lower limits varied between approximately ± 4dB.
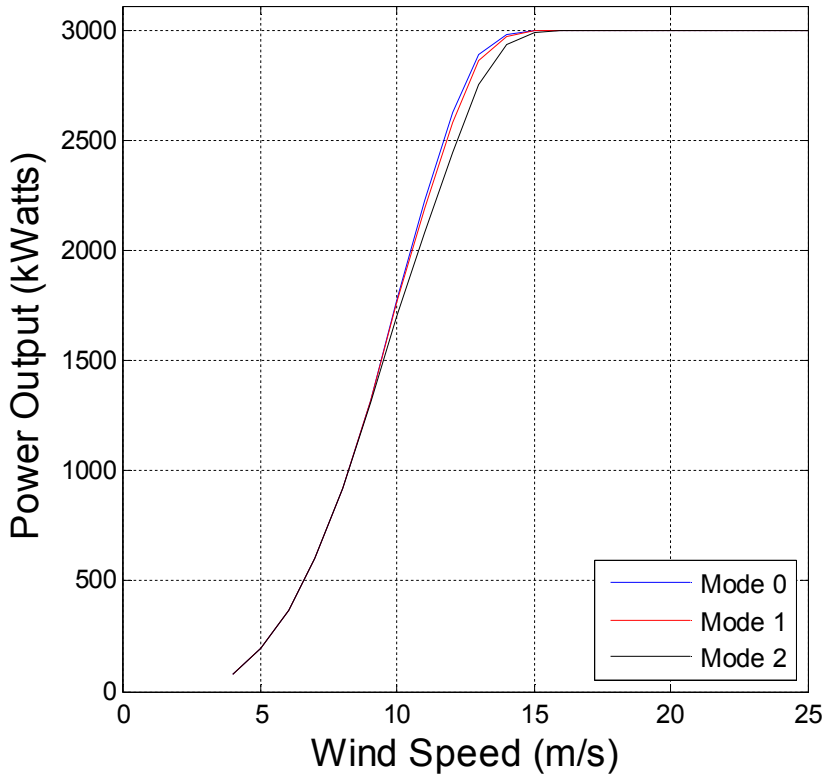
Spectral measurements at monitoring station HC1P, located nearest to the Summerside V-90 turbines, display a ramping up of the ground motion energy with a particular pattern that resembles the power output curves of the Vestas 3.0 MW V-90 provided in the turbines' general specifications (Vestas, 2006, Fig. 21). This is to be anticipated as the noise output by the turbines at these frequencies is related to the rotational rate of the turbine blades, which are moderated by a combination of the turbine's rotor and the blade pitch to produce electrical power between rotor speeds of 9.9 - 18.4 RPM with a nominal speed of 16.1 RPM. To examine the quality of the fit of the three Vestas operating output curves to the observed ground motion, the shape of the operating curves (as provided by the V-90 general specifications) are least squares fit to the RMS ground motion amplitude data using three unknown scaling terms.

$$F(w) = A\frac{P_{\text{mode}}(w+B)}{P_{peak}} + C$$
(2)

where fitted unknowns A, B and C are a vertical scaling term, a wind correction or horizontal shifting term (also measure of how accurately the winds from 10m height were extrapolated to the hub height of 80 m) and a DC offset term, respectively. P_{mode} and P_{peak} represent the turbine power mode at the specific wind speed, w, and the peak turbine output power (3.0 MW) respectively. Results of fitting the three modes showed that Mode 2 was consistently a better fit than either Mode 0 or Mode 1 for nearly all frequencies (Table 5). At this time it is unknown as to which mode the Summerside V-90 turbines were operating under during the course of the deployment.

Overall the general quality of fit to the measured frequencies features at 1.61, 2.41, 3.22, 4.03, and 4.83 Hz is excellent reaching R-squared values exceeding 0.99, where a value of 1.0 would indicate a perfect fit to the measured data (Table 5, Fig. 22). The quality of this fit reinforces the interpretation that the peaks at these frequencies result from harmonics of the turbine blades, since the mitigating factor for the power output of the turbine blades should be that of the turbine generator to which they are attached. Using the same turbine operating functions to fit the spectral features associated with the tower bending and torsional modes at 2.50, 3.50 and 5.82 Hz, result in a somewhat poorer quality of fit than those of the blade pass harmonics, which may imply that the blades passing near the tower may again not be the only stimulus in exciting these frequencies. Many forces, besides the turning of the turbine blades, are likely exerted either directly or indirectly on the tower causing the tower to bend, even during light wind conditions.
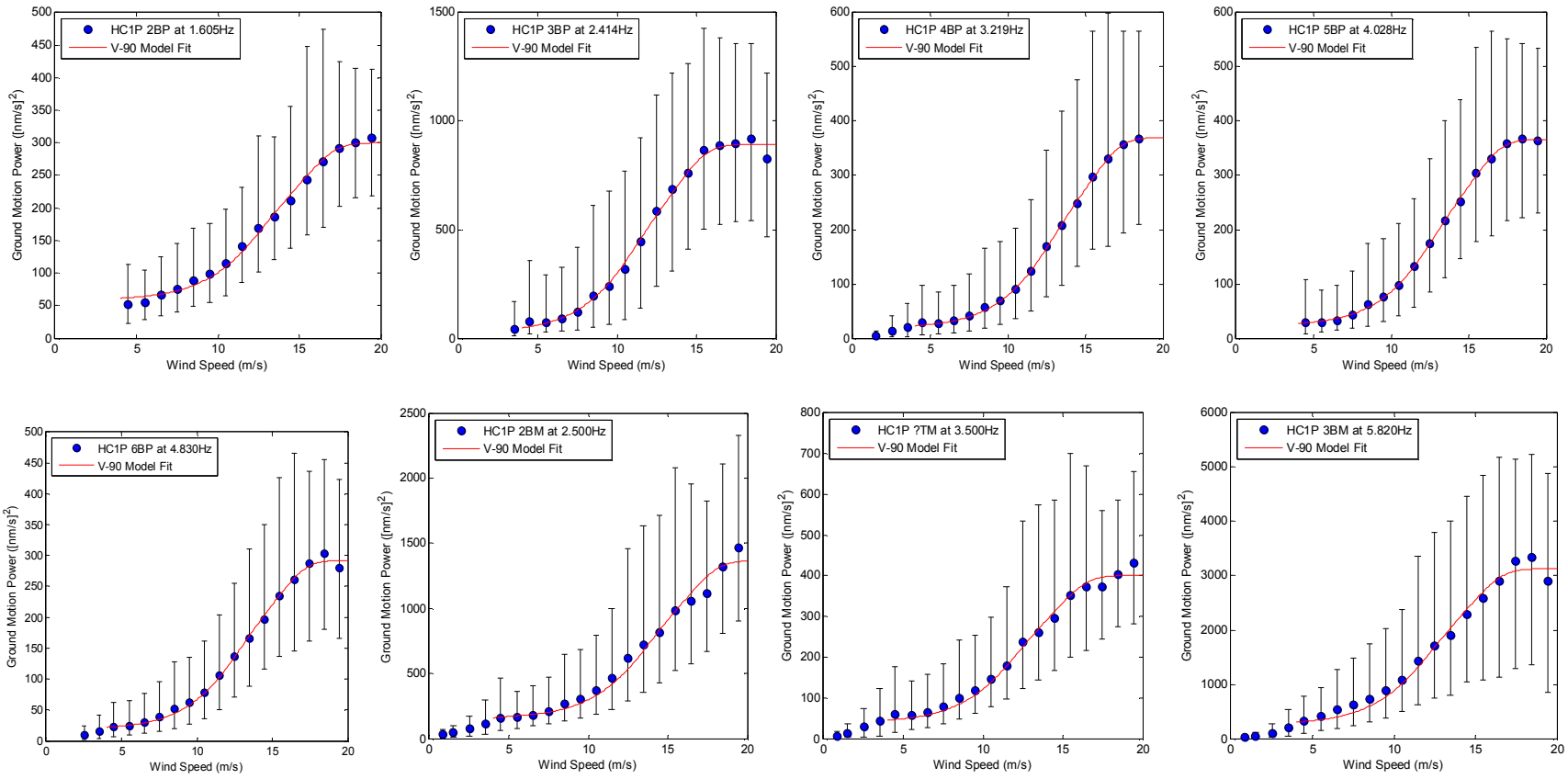
Finally it is noted that consistently a shift of 3.5 ± 0.7 m/s was needed to align the V-90 specification curves to the observed data. This suggests that nacelle winds at a height of 80m were somewhat over-estimated by equation (1) and that a slightly smaller Hellman or wind shear exponent in equation (1) is necessary (closer to 0.2) to match actual winds at the V-90 Hub height with the extrapolated winds measured at 10m. Ideally measured winds from the turbine nacelle could be used to confirm this supposition, should they be made available in the future.

Fig. 21: Vestas 3.0MW V-90 wind turbine operating modes as provided in the general specifications of the manufacturer for the turbine operating near sea level (air density: 1.27 kg/m^3). Modes are similar with minor variations in power output between 9 to 15 m/s wind speeds. Peak power output of 3.0 MW is reached at a speed of 17 m/s by all modes. Power output behaviour below 4 m/s is not provided in the general specifications (Vestas, 2006).

Association	Frequency (Hz)	Scaling	Wind Offset (m/s)	DC Offset (nm/s)^2	R-squared Fit
2BP	1.61	231.7	3.74	68.3	0.9947
3BP	2.41	831.4	2.18	61.4	0.9955
4BP	3.22	336.6	3.80	33.2	0.9994
5BP	4.03	330.0	3.63	36.6	0.9994
6BP	4.83	262.6	3.73	29.7	0.9968
2BM	2.50	1161.2	4.70	204.8	0.9855
?TM	3.50	347.2	3.06	53.6	0.9903
3BM	5.82	2758.1	3.19	372.5	0.9853

Table 5: Vestas V-90 wind Mode 2 power output curve fit to ground motion power data measured at monitoring station HC1P as a function of increasing wind speed for both blade-pass harmonics and turbine tower modes.

Fig. 22: Fitting results for the Vestas 3.0MW V-90 operating power Mode 2 to the RMS ground motion power measurements made from spectral data at narrow frequency bands associated with blade pass harmonics and tower bending/torsional modes. (top – left to right) 2BP at 1.61 Hz, 3BP at 2.41 Hz, 4BP at 3.22 Hz, and 5BP at 4.03 Hz. (bottom left to right) 6BP at 4.83 Hz, 2BM at 2.50 Hz, ?TM at 3.50 Hz and 3BM at 5.82 Hz. Bars on each data point represent positions of 25th and 75th percentile measurements.

32

4.1 Seismic Propagation and Attenuation of Turbine Noise

The inner-quartile mean spectra computed, measured and discussed in the preceding section (Fig. 17-20, Tables 6-9) provide the constraints to the analysis that will be described here. Although these measurements represent the observations of seismic ground motion generated by all four of the Summerside Vestas V-90 wind turbines operating normally, as opposed to measuring that of a single turbine, it is useful to discuss the development of a propagation and attenuation model from the view of a single turbine. It will then be shown how this model can be extended to noise from multiple turbines.

The spectral amplitude for the far field noise of a single turbine as measured at any arbitrary position, A, is the product of a turbine's noise source function, T, and the attenuation of the source function due to geometrical spreading and any anelastic attenuation due to the properties of the medium in which the seismic waves are propagating.

$$A(f, R, w) = T(f, w) \, P(f, R) \tag{3}$$

where f is the frequency, R is the distance measured from the base of the turbine, and w is the speed of the wind acting on the turbine blades. Here the assumption is made that the turbine acts as an isotropic source and so the source function will have no directional dependence. A similar assumption is also made regarding the propagating medium in that there is no azimuthal anisotropy in attenuation.

With these assumptions, the seismic attenuation function, P, can be expressed as a function of distance, R, and frequency, f:
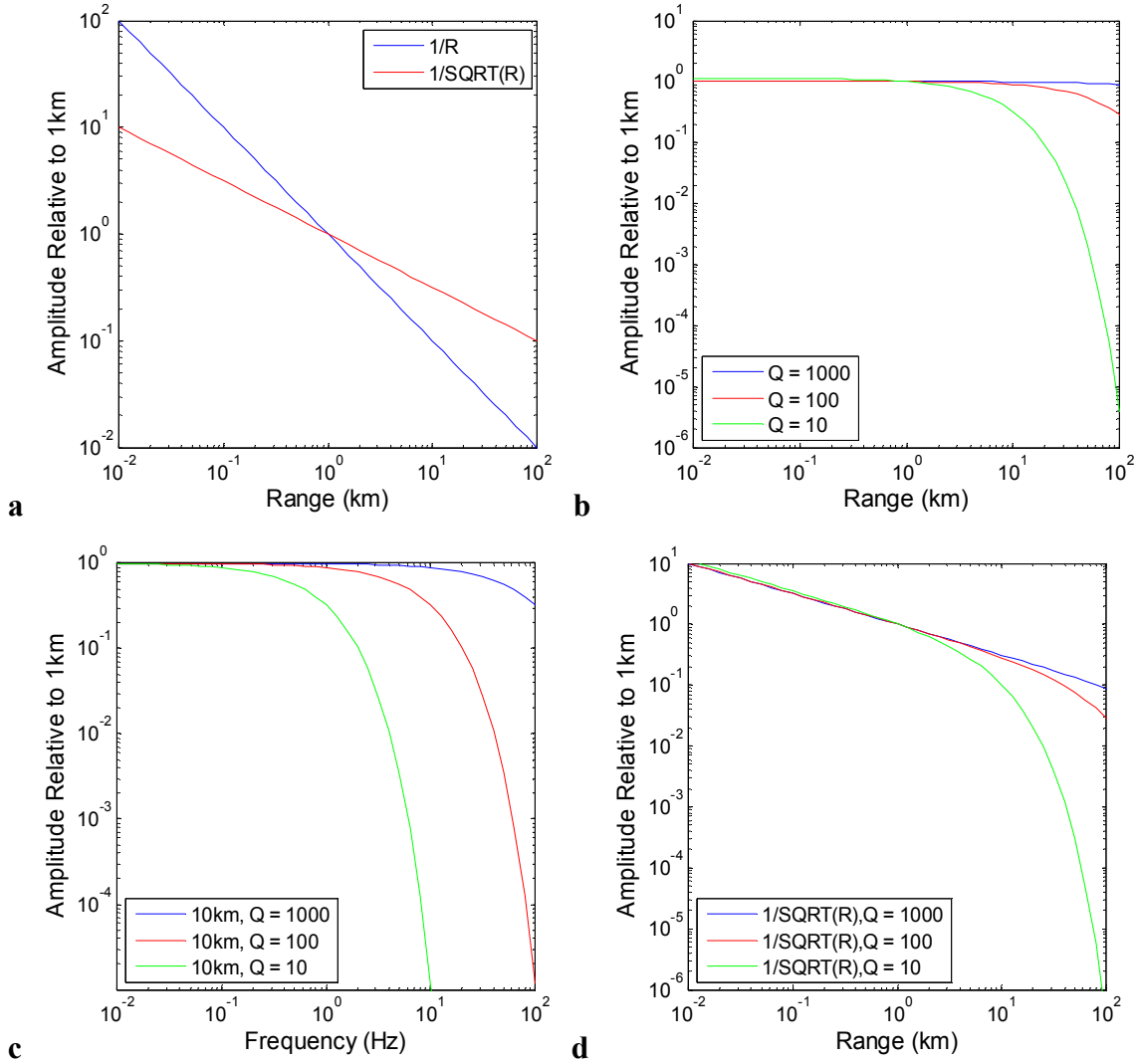
$$P(f, R) = \left(\frac{R}{R_0} \right)^{-\beta} \exp\left(-\frac{\pi f (R - R_0)}{vQ} \right) \tag{4}$$

where R_0 is a reference distance from the source, β is the geometrical spreading exponent, v is the velocity of the propagating seismic waves and Q is the quality factor and a measure of the anelastic absorption of seismic energy by the medium.

The first factor in (4) represents the attenuation due to geometrical spreading. The exponent β in this expression determines the rate of this attenuation and is dependent upon the type of seismic waves being generated. For seismic body waves generated by subsurface sources, geometrical spreading of the amplitude attenuates with an exponent of $\beta = 1$, where for surface waves such as Rayleigh or Love waves $\beta = \frac{1}{2}$. Thus surface waves attenuate more slowly than do seismic body waves (Fig. 23a).

The second factor in (4) represents additional attenuation due to the anelastic properties of the propagating medium, specifically unequal absorption of higher frequencies. Characterized by the quality factor, Q, typical values for competent bedrock tend to be quite large (e.g. 500+) representing the ease with which high frequencies may be transmitted through rock, while values for soils and uncompacted sediments tend to be low, due to poor transmission of high frequencies through loose soil grains. In North America, soils have shown measured quality values to range

33

between ~10 – 50 (e.g. Campbell 2009, Gibbs et al. 1994). The effect of different values of Q, both in range and frequency is shown in Figs. 23b/c. The combined effect of both geometrical and anelastic attenuation can be seen in Fig. 23d, where close to the source and/or with large values of Q, geometrical spreading dominates the attenuation, while at distance and/or at higher frequencies the effects of anelastic absorption can be seen.

Fig. 23: Seismic attenuation of amplitude. a) Attenuation by geometrical spreading typical for seismic body waves (blue) and surface waves (red) normalized at a range of 1 km. b) Anelastic absorption with distance for a range of quality factors. c) Anelastic absorption as a function of frequency at a distance of 10 km. d) Total attenuation as the product of geometrical and anelastic absorption as a function of range for a 1 Hz surface wave.

To determine the type of attenuation most applicable to that of the Summerside V-90 turbines, a comparison is made between the measured turbine-induced ground motions and possible attenuation properties. As power, or energy, is proportional to the square of amplitude, the

attenuation function (4) is similarly squared resulting in a ground motion power function (Bowers, 2013) of:

$$g(f,w,R) = \left[T(f,w)\left(\frac{R}{R_0}\right)^{-\beta} \exp\left(-\frac{\pi f(R-R_0)}{vQ}\right) \right]^2 \qquad (5)$$

When the measurements of spectral power for the 3BP – 6BP and 2BM frequencies (observed on either all four or the nearest three monitoring stations) are compared with typical body wave and surface wave attenuation (Fig 24), it is seen that surface wave attenuation fits the observations best. This agrees with findings and hypotheses of previous studies of wind turbine noise, having fewer distance-distributed stations and observing a variety of wind turbines, as sources of surface or Rayleigh waves (Bowers 2013, Saccorotti et al. 2011, and Styles et al. 2005).

It is also noted that no additional curvature to the surface wave attenuation is observed over the blade-pass harmonics measured (Fig. 25) suggesting that the quality factor of the medium in which the waves are travelling is quite high (>1000). A high quality factor suggests that the surface waves are travelling in a hard, competent medium that would more easily allow transmission of higher frequencies as opposed to the types of soils observed by Gibbs et al. (1994), Campbell (2009) and used by Schofield (2002). Geotechnical documents from the construction of the Summerside turbines suggest that poor quality, loose soils were discovered in the area and required using either pile foundations or gravity base foundations for the turbines on either compacted gravel or directly on excavated bedrock at approximately 6-7 m depth (AMEC Earth & Environmental, 2009). The latter case would provide direct coupling of vibrations to the sandstone bedrock. With the relatively shallow depth of bedrock in the area, the measurements of the attenuation at higher blade-pass frequencies suggest that the surface waves generated by the sway and vibration of the turbines propagates primarily through the sandstone bedrock and not through upper soil layers. With this information, the attenuation model parameter values of (3) are chosen to reflect the propagation of surface waves through local bedrock using a high quality factor (Q) of 1000, with a surface wave group speed (v) of 2.4 km/s (e.g. Styles 2010, Bowers, 2013) at a reference distance (R_o) of 1.0 kilometer.

Mode		2BP	3BP	4BP	5BP	6BP	2BM	?TM	3BM
Peak Frequency (Hz)	**IQM Wind Speed**	1.61	2.41	3.22	4.03	4.83	2.50	3.50	5.82
Freq. Band (Hz)	**m/s**	1.58 – 1.64	2.37 – 2.45	3.17 – 3.28	3.97 – 4.08	4.77 – 4.89	2.45 – 2.58	3.40 – 3.59	5.70 – 6.00
	0.86	----	----	----	----	----	31.033	6.887	19.718
	1.52	----	----	4.323	----	----	45.476	13.525	44.849
	2.52	----	----	12.33	----	8.832	75.802	28.433	96.862
	3.52	----	43.331	20.125	----	14.811	113.162	43.031	195.123
	4.49	51.795	74.731	28.435	29.066	22.391	160.012	59.243	322.133
	5.51	55.296	72.326	26.754	28.147	24.629	161.915	56.439	419.946
	6.51	66.036	88.42	31.816	33.132	29.792	182.572	64.825	534.858
	7.51	74.996	122.627	41.001	43.83	38.056	208.026	77.819	620.884
	8.48	87.853	193.317	57.411	62.316	51.642	268.42	98.743	735.517
	9.51	98.346	240.845	70.082	75.751	62.041	303.589	117.69	893.597
	10.48	115.05	315.926	90.827	97.528	78.788	366.113	146.072	1070.899
	11.47	141.089	443.412	122.88	132.084	106.344	465.736	178.424	1427.756
	12.49	169.336	587.26	169.101	175.262	137.19	620.715	237.732	1710.975
	13.46	186.366	687.299	207.726	216.512	165.845	719.805	261.746	1898.414
	14.46	210.916	759.555	248.053	252.624	197.166	818.059	296.612	2298.228
	15.49	243.073	866.354	297.195	304.486	234.314	984.69	351.366	2579.236
	16.49	271.21	887.367	330.167	330.18	260.602	1058.148	373.394	2904.615
	17.46	291.734	897.271	357.157	359.032	287.471	1111.898	373.297	3267.872
	18.45	300.503	918.488	367.275	367.416	303.961	1316.702	403.778	3350.033
	19.45	307.338	827.598	----	363.749	280.554	1465.171	430.699	2899.915

Table 6. HC1P power measurements of ground motion associated with blade-pass harmonics and tower bending modes as a function of wind speed. Measurements have units of velocity (nanometers per second) squared or $(nm/s)^2$.

Mode		3BP	4BP	5BP	6BP	7BP	2BM	?TM
Peak Frequency (Hz)	IQM Wind Speed	2.41	3.22	4.03	4.83	5.64	2.50	3.50
Freq. Band (Hz)	m/s	2.37 – 2.45	3.17 – 3.28	3.97 – 4.08	4.77 – 4.89	5.57 – 5.69	2.45 – 2.58	3.40 – 3.59
	0.86	----	----	----	----	----	6.823	2.245
	1.52	----	----	----	----	----	9.322	3.629
	2.52	----	4.568	----	2.885	2.476	13.371	6.998
	3.52	----	5.215	3.638	3.166	2.823	16.976	8.125
	4.49	11.854	6.844	4.631	3.997	3.576	21.774	10.581
	5.51	12.499	7.369	5.122	4.48	3.929	22.313	10.872
	6.51	13.457	8.195	5.742	4.972	4.397	23.463	11.69
	7.51	16.399	10.184	7.206	6.168	5.342	27.423	13.829
	8.48	20.782	12.152	8.746	7.369	6.442	32.504	15.779
	9.51	25.158	14.311	10.045	8.53	7.652	37.348	18.106
	10.48	31.848	18.806	13.219	11.505	10.038	45.7	23.456
	11.47	40.941	22.52	16.664	14.674	12.97	54.489	27.388
	12.49	50.856	27.858	20.289	18.338	16.171	68.109	33.754
	13.46	61.267	35.634	25.811	23.202	21.375	82.778	43.273
	14.46	71.916	42.61	32.154	28.894	26.942	98.82	52.303
	15.49	85.551	52.654	41.22	37.633	37.351	126.045	----
	16.49	106.069	71.845	58.918	54.367	54.235	151.749	----
	17.46	133.906	92.211	75.616	70.618	70.364	189.707	----
	18.45	157.22	122.879	95.779	84.526	89.041	249.461	----
	19.45	269.608	----	217.542	196.84	----	443.725	----
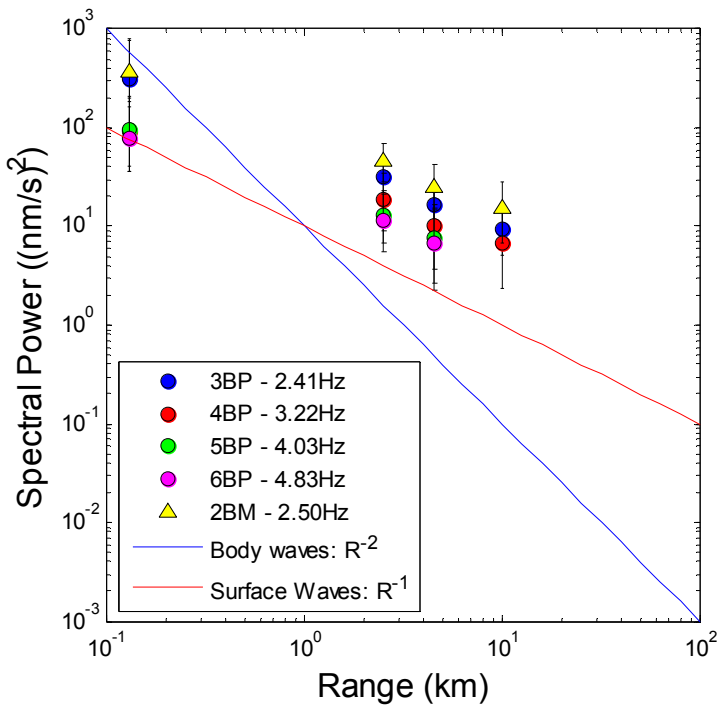
Table 7. HC2P power measurements of ground motion associated with blade-pass harmonics and tower bending modes as a function of wind speed. Measurements have units of velocity (nanometers per second) squared or $(nm/s)^2$.

Mode		3BP	4BP	5BP	6BP	7BP	2BM
Peak Frequency (Hz)	IQM Wind Speed	2.41	3.22	4.03	4.83	5.64	2.50
Freq. Band (Hz)	m/s	2.37 – 2.45	3.17 – 3.28	3.97 – 4.08	4.77 – 4.89	5.57 – 5.69	2.45 – 2.58
	0.86	----	----	----	----	----	4.689
	1.52	----	----	----	----	----	6.067
	2.52	----	----	----	----	----	9.22
	3.52	6.811	4.628	3.829	----	----	11.591
	4.49	8.814	6.023	4.814	----	----	14.851
	5.51	8.883	6.206	4.845	----	----	14.832
	6.51	9.397	6.277	4.872	----	----	15.158
	7.51	11.072	7.056	5.784	5.254	4.117	17.325
	8.48	12.786	7.546	6.124	5.422	4.404	19.673
	9.51	14.092	8.252	6.502	5.612	4.456	21.301
	10.48	16.685	10.269	7.696	6.819	5.26	25.372
	11.47	18.607	10.855	8.124	7.384	5.515	26.958
	12.49	21.876	11.932	9.053	8.413	6.137	30.919
	13.46	24.126	13.379	9.858	8.878	6.648	35.07
	14.46	28.181	16.586	11.701	11.152	8.318	40.858
	15.49	32.994	18.705	13.796	12.334	9.094	48.436
	16.49	30.762	15.481	11.574	9.726	7.799	44.025
	17.46	31.753	14.893	11.666	9.412	7.678	45.776
	18.45	33.084	17.564	12.127	10.363	8.343	50.938
	19.45	35.208	20.738	14.695	----	----	60.632
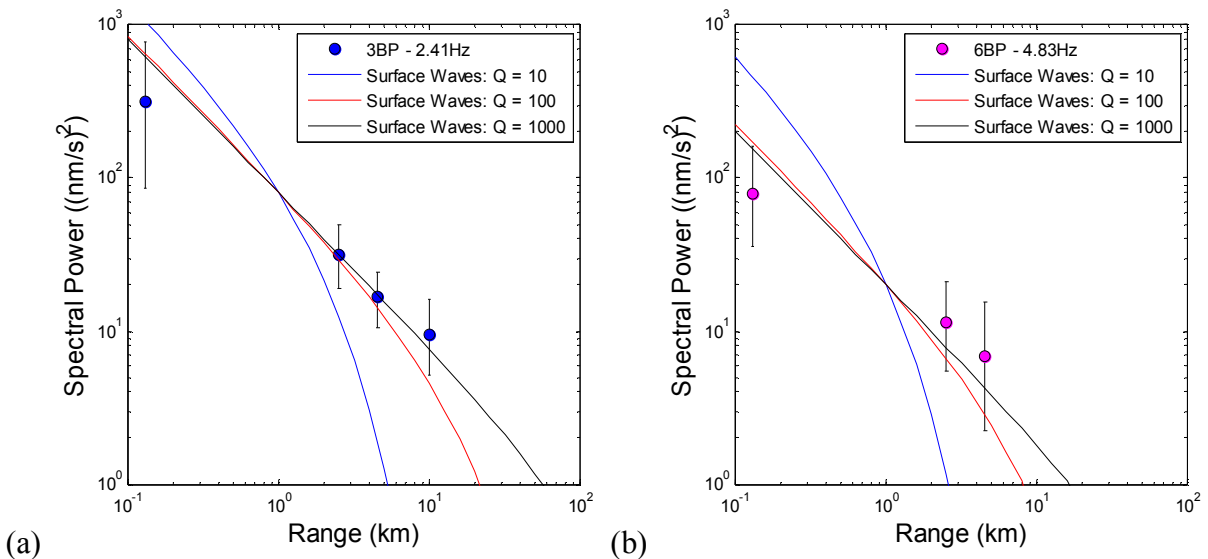
Table 8. HC3P power measurements of ground motion associated with blade-pass harmonics and tower bending modes as a function of wind speed. Measurements have units of velocity (nanometers per second) squared or $(nm/s)^2$.

Mode		3BP	4BP	2BM
Peak Frequency (Hz)	IQM Wind Speed	2.41	3.22	2.50
Freq. Band (Hz)	m/s	2.37 – 2.45	3.17 – 3.28	2.45 – 2.58
	0.86	----	----	----
	1.52	----	----	----
	2.52	----	----	----
	3.52	----	----	----
	4.49	----	----	----
	5.51	----	----	----
	6.51	----	----	----
	7.51	7.045	----	11.247
	8.48	7.494	5.252	11.893
	9.51	8.064	5.552	12.69
	10.48	9.457	6.838	15.143
	11.47	9.815	7.06	15.147
	12.49	10.466	7.377	16.214
	13.46	11.576	8.369	17.504
	14.46	13.054	10.128	20.372
	15.49	14.319	10.847	22.363
	16.49	13.201	9.667	19.46
	17.46	12.878	8.807	19.199
	18.45	12.627	8.383	18.824
	19.45	14.825	10.184	22.384

Table 9. HC4P power measurements of ground motion associated with blade-pass harmonics and tower bending modes as a function of wind speed. Measurements have units of velocity (nanometers per second) squared or $(nm/s)^2$.

Fig. 24: Comparison of measured attenuation as a function of range with theoretical attenuation of seismic body waves and surface waves. Observed attenuation more closely matches that of surface wave attenuation, suggesting that the turbines act as a source of surface waves with tonal frequencies.


Fig. 25: Comparison of measured turbine noise peaks at high and low frequencies to least squares fitted surface wave attenuation with anelastic attenuation with varying quality factors. Measurements indicate quality factors of surface are quite high (>1000) as no significant anelastic attenuation is observed within measurement uncertainty. (a) 3BP harmonic 2.41 Hz (b) 6BP harmonic at 4.83 Hz.

4.2 Multiple vs. Single Turbine Noise

The measurements of noise made in Tables 6-9 represent the noise of not one but four individual Vestas 3.0MW V-90 turbines, with each turbine located at a different distance from the station of measurement. Thus the noise spectrum power measured is actually a sum of the contributions of each turbine's noise power. Following Bowers (2013), if N identical turbines are assumed to be each an isotropic source, and are rotating at a random phase to each other at a distance r_k, from the monitoring site, then the noise power, T, of each turbine, k, will sum as:

$$G(f,w) = \frac{1}{N} \sum_{k=1}^{N} T_k(f,w) \left[\left(\frac{r_k}{R_0} \right)^{-\frac{1}{2}} \exp\left(-\frac{\pi f (r_k - R_0)}{vQ} \right) \right]^2 \qquad (6)$$

Thus the observed turbine noise can be thought of as a weighted sum of the turbine noise spectra, where the weight for each turbine spectrum is determined by the attenuation experienced due to its distance from the observer.

The total RMS ground motion induced by these turbines, for any specific wind speed, will then be the square root of the integral of (6) over the frequency pass band of interest which contains the turbine noise or:

$$RMS(w) = \sqrt{\int_{f_1}^{f_2} G(f,w) df} \qquad (7)$$

From equation (6) and the chosen attenuation model parameters from Section 4.1, these weights can be determined given that the positions and distances of the Summerside turbines from each station are known (Table 1). Shown in Table 10, it is seen that Turbine #2 contributes nearly 60% of the contribution of the noise observed at HC1P due to its proximity the station, with the remaining contributed by another ~20% by Turbine #4 and nearly equal parts, #1 and #2. In contrast, stations HC2P, HC3P and HC4P show increasingly equal contributions from all turbines as the observation distance becomes significantly larger than the individual turbine separations.

If the assumptions that each of the four turbines generate identical noise spectra under similar wind conditions, and that the four Summerside turbines are sufficiently close together that each of the turbine experienced the same wind conditions, then an equivalent distance, r_0, can be calculated that reflects where the observed spectrum at a monitoring station would equal that of a single turbine or:

$$\left[\left(\frac{r_0}{R_0} \right)^{-\frac{1}{2}} \exp\left(-\frac{\pi f (r_0 - R_0)}{vQ} \right) \right]^2 = \frac{1}{N} \sum_{k=1}^{N} \left[\left(\frac{r_k}{R_0} \right)^{-\frac{1}{2}} \exp\left(-\frac{\pi f (r_k - R_0)}{vQ} \right) \right]^2 \qquad (8)$$

Although (6) is nonlinear due to the anelastic attenuation factor, the contribution of anelasticity is negligible in the model, contributing << 1% to total attenuation and thus in (8) may be treated as

~1. Without significant anelasticity, (8) becomes frequency independent. Solving (8) for the four monitoring stations, the equivalent distances for a single turbine asymptotically approach the mean turbine distance as the station's range from the facility increases (Table 11).

Station	Contribution to observed power spectrum (%)			
	Turbine #1	Turbine #2	Turbine #3	Turbine #4
HC1P	12.01%	58.71%	10.10%	19.19%
HC2P	22.46%	27.02%	26.03%	24.49%
HC3P	23.63%	26.29%	25.30%	24.78%
HC4P	24.32%	25.60%	25.19%	24.89%

Table 10: Relative contributions of the four Summerside Vestas V-90 wind turbines to the observed spectra at the four monitoring stations assuming the turbines are isotropic surface wave sources and the blades are rotating in random phase to each other.

Station	Turbine #1	Turbine #2	Turbine #3	Turbine #3	Mean Distance	Single Turbine
	km	km	km	km	km	km
HC1P	0.634	0.130	0.753	0.397	0.478	0.305
HC2P	3.031	2.527	2.622	2.784	2.741	2.728
HC3P	5.053	4.557	4.730	4.826	4.791	4.785
HC4P	10.561	10.067	10.219	10.337	10.296	10.293

Table 11: Distances of seismo-acoustic monitoring stations to the various Summerside wind turbines compared to the equivalent single turbine distance.

4.3 Estimated RMS Noise within Turbine Observation Band

While measurement of the growth and decay of individual spectral peaks and harmonics are important to determine the likelihood of observation/detection of the turbine source as a function of distance, it does not necessarily address how these features affect the broadband ground motion observed at these sites. To determine the contribution of the turbine noise to the overall broadband ground motion within which it is observed, the ambient background noise level, without turbine noise, is estimated using the computed inner-quartile mean power spectral density (PSD) at each station. After background estimation, the root mean square (RMS) levels of the background and the background + turbine noise are computed by integration of the inner-quartile mean PSD from frequencies of 0.8 Hz to 10.0 Hz then taking the square root. This spectral band is located slightly higher than the microseism band and encompasses the observed far-field turbine noise. This band is also similar to the monitoring band used for regional earthquake observation and location for later comparison.

To estimate the behavior of the ambient background, data from each inner-quartile mean PSD for stations HC2P, HC3P and HC4P were least squares fit (after muting spectral peaks associated with the Summerside wind turbines) between frequencies of 0.8 Hz and 10 Hz using a 7th order

polynomial of the form:
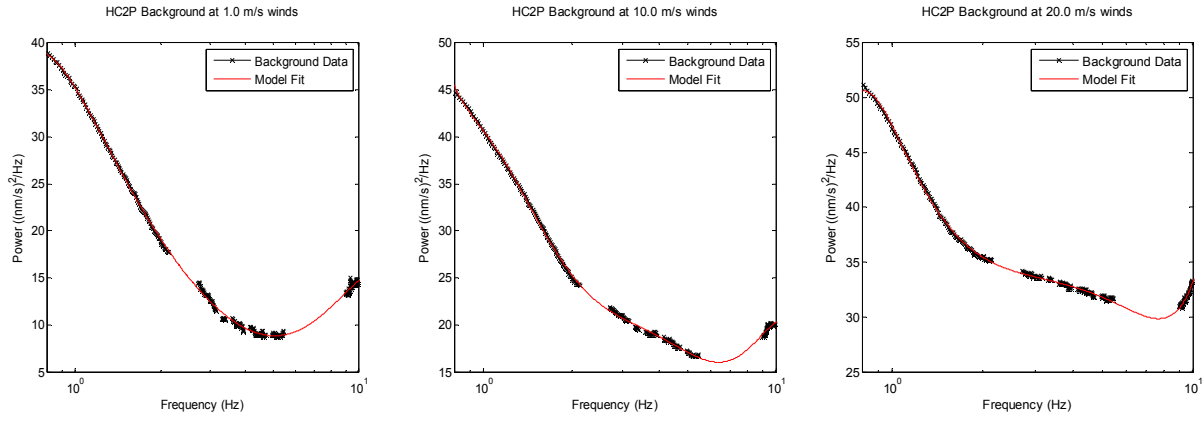
$$\log_{10}(N(f)^2) = A_0 + A_1*\log_{10}(f) + A_2*\log_{10}^2(f) + \ldots + A_7*\log_{10}^7(f) \tag{9}$$

where $N(f)^2$ is the spectral power in nm/s, and f is the frequency in Hz.

It is noted that monitoring station HC1P's background could not be estimated directly because of the presence of the nearly continuous peaks likely associated to the turbine tower at frequencies >5 Hz (Fig. 17) due to its proximity to turbine #2. Instead as a proxy to HC1P's ambient background, the fitted background associated with the nearest monitoring station, HC2P, is used. Coefficient fits to the three more distant monitoring stations are provided in Tables 12-14 and examples of typical fits for station HC2P in Fig. 26.

HC2P								
Wind Speed (m/s)	A_0	A_1	A_2	A_3	A_4	A_5	A_6	A_7
0 − 1	35.25	-48.82	-84.47	366.4	-575.2	221.1	-79.4	-41.3
1 − 2	35.30	-45.31	-48.70	-99.8	1348.5	-1509.5	2747.0	-902.2
2 − 3	36.29	-47.35	-61.47	-88.6	1873.6	-2296.8	4362.8	-1464.3
3 − 4	37.54	-47.42	-42.82	-308.1	2641.1	-2916.5	5322.4	-1752.1
4 − 5	38.47	-46.23	-50.93	-301.4	2699.2	-2987.4	5434.0	-1780.0
5 − 6	38.84	-45.39	-34.14	-430.5	3003.3	-3130.3	5515.9	-1768.8
6 − 7	39.42	-43.71	-30.60	-525.3	3323.2	-3349.9	5780.7	-1825.2
7 − 8	39.78	-42.26	-30.95	-569.5	3519.5	-3511.8	6005.8	-1879.3
8 − 9	40.15	-41.83	-22.53	-609.1	3560.2	-3495.6	5934.8	-1850.7
9 − 10	40.64	-41.55	-28.51	-576.6	3496.6	-3474.7	5943.8	-1864.8
10 − 11	41.51	-41.74	-46.72	-452.8	3186.6	-3276.3	5674.9	-1788.1
11 − 12	42.29	-40.26	-48.43	-501.1	3361.8	-3385.3	5776.8	-1798.6
12 − 13	42.85	-42.28	-70.09	-224.9	2412.8	-2648.1	4693.0	-1492.3
13 − 14	43.51	-43.13	-81.64	-114.0	2077.1	-2388.6	4275.5	-1356.0
14 − 15	43.97	-44.64	-91.54	31.3	1578.6	-1998.4	3692.4	-1188.3
15 − 16	44.48	-46.57	-82.52	114.2	1085.9	-1497.4	2799.1	-892.9
16 − 17	45.32	-49.07	-91.18	349.1	121.4	-645.9	1406.9	-462.9
17 − 18	46.42	-52.12	-105.29	600.7	-783.7	61.4	378.4	-178.5
18 − 19	46.84	-53.16	-92.46	662.0	-1229.1	534.9	-493.7	119.9
19 − 20	47.46	-53.24	-84.58	960.8	-2658.0	1849.7	-2701.3	822.6

Table 12: Ambient background noise modelling coefficients for monitoring station HC2P as a function of wind speed.

Fig. 26: Example of polynomial fits to seismic background for HC2P at 0 – 1.0 m/s (left), 9 – 10 m/s (middle) and 19 – 20 m/s (right) wind speeds within the 0.8 – 10 Hz frequency band. Segments of spectrum displaying turbine spectral peaks are muted prior to fit.

HC3P							
Wind Speed (m/s)	A_0	A_1	A_2	A_3	A_4	A_5	A_6	A_7
0 – 1	35.13	-48.29	-64.62	55.2	726.7	-955.8	1925.1	-702.4
1 – 2	35.27	-46.00	-50.69	-177.9	1853.4	-2068.2	3851.2	-1313.4
2 – 3	36.12	-47.43	-53.14	-287.4	2817.9	-3218.3	6026.7	-2039.4
3 – 4	37.40	-48.68	-45.67	-297.9	2688.4	-3013.7	5598.8	-1888.3
4 – 5	38.26	-46.55	-43.29	-437.3	3326.2	-3599.6	6562.1	-2182.9
5 – 6	38.57	-45.35	-30.39	-557.7	3639.4	-3781.9	6756.7	-2220.2
6 – 7	39.17	-43.93	-23.63	-662.0	3939.6	-3967.6	6969.0	-2265.9
7 – 8	39.45	-42.00	-24.10	-726.0	4205.0	-4179.7	7267.0	-2342.8
8 – 9	39.83	-41.18	-12.40	-804.6	4367.8	-4251.8	7314.9	-2343.4
9 – 10	40.29	-41.47	-20.30	-738.5	4156.3	-4088.7	7068.8	-2270.5
10 – 11	41.10	-40.69	-36.10	-718.2	4307.0	-4320.8	7541.3	-2435.2
11 – 12	41.93	-39.05	-31.57	-862.6	4827.9	-4709.8	8072.6	-2571.7
12 – 13	42.44	-40.44	-42.10	-732.2	4365.6	-4331.5	7483.4	-2395.6
13 – 14	43.10	-40.19	-49.29	-783.2	4748.1	-4745.2	8230.9	-2640.6
14 – 15	43.57	-42.69	-62.96	-551.0	3900.2	-4055.2	7167.0	-2324.5
15 – 16	44.04	-43.74	-70.04	-487.5	3782.0	-4030.9	7208.3	-2352.1
16 – 17	44.78	-46.82	-80.49	-395.1	3430.9	-3713.8	6682.2	-2190.4
17 – 18	45.76	-48.99	-98.01	-310.9	3305.9	-3701.9	6772.5	-2245.7
18 – 19	46.04	-49.28	-81.60	-453.3	3812.8	-4122.0	7418.3	-2431.1
19 – 20	46.65	-50.09	-97.98	-406.5	3955.4	-4410.5	8048.3	-2655.8

Table 13: Ambient background noise modelling coefficients for monitoring station HC3P as a function of wind speed.

44

HC4P							
Wind Speed (m/s)	A_0	A_1	A_2	A_3	A_4	A_5	A_6	A_7
0 − 1	35.48	-57.80	-119.94	1070.7	-3848.0	3692.1	-6762.1	2306.8
1 − 2	35.61	-57.09	-117.01	1062.1	-3659.8	3369.2	-6009.3	2017.0
2 − 3	36.50	-57.87	-110.06	865.7	-2464.7	2039.9	-3515.7	1177.4
3 − 4	37.73	-57.64	-96.77	689.4	-1905.9	1646.2	-2988.6	1040.7
4 − 5	38.59	-55.63	-98.23	563.2	-1310.7	1092.7	-2062.1	751.1
5 − 6	38.93	-54.19	-87.37	404.7	-711.2	579.0	-1233.8	496.7
6 − 7	39.56	-52.45	-82.96	305.6	-427.4	410.8	-1051.9	459.5
7 − 8	39.80	-51.02	-74.84	189.4	-37.4	126.6	-675.5	368.4
8 − 9	40.18	-49.77	-58.21	10.5	526.3	-282.6	-106.6	215.0
9 − 10	40.65	-49.28	-65.51	20.9	545.4	-318.9	-23.9	181.8
10 − 11	41.45	-47.67	-81.17	-67.7	1326.5	-1225.0	1682.2	-391.1
11 − 12	42.21	-45.03	-71.93	-288.9	2100.4	-1801.6	2484.5	-605.3
12 − 13	42.74	-45.85	-77.70	-270.9	2114.4	-1849.0	2593.2	-644.9
13 − 14	43.39	-45.41	-84.40	-345.2	2621.1	-2392.8	3579.2	-969.4
14 − 15	43.91	-47.34	-102.03	-221.3	2444.0	-2425.9	3849.7	-1101.2
15 − 16	44.53	-48.23	-111.46	-179.6	2425.1	-2490.3	4055.1	-1190.3
16 − 17	45.20	-50.20	-117.06	-128.2	2132.8	-2143.0	3360.9	-942.8
17 − 18	46.04	-52.35	-114.00	-171.6	2232.6	-2148.9	3245.1	-873.3
18 − 19	46.51	-53.19	-116.26	-154.3	2106.6	-1985.7	2907.5	-750.9
19 − 20	47.16	-54.68	-137.02	-9.3	1842.6	-1938.1	3046.6	-843.9

Table 14: Ambient background noise modelling coefficients for monitoring station HC4P as a function of wind speed.

Once estimates of the ambient background spectrum are obtained, comparison of the added contribution of the turbine spectral noise to the 0.8 − 10.0 Hz spectral band is possible. For each monitoring station and wind speed category, the ambient background and the measured IQM spectra are integrated within the aforementioned passband and the square root taken to provide nominal values for the resulting time domain RMS ground motion levels (Table 15).
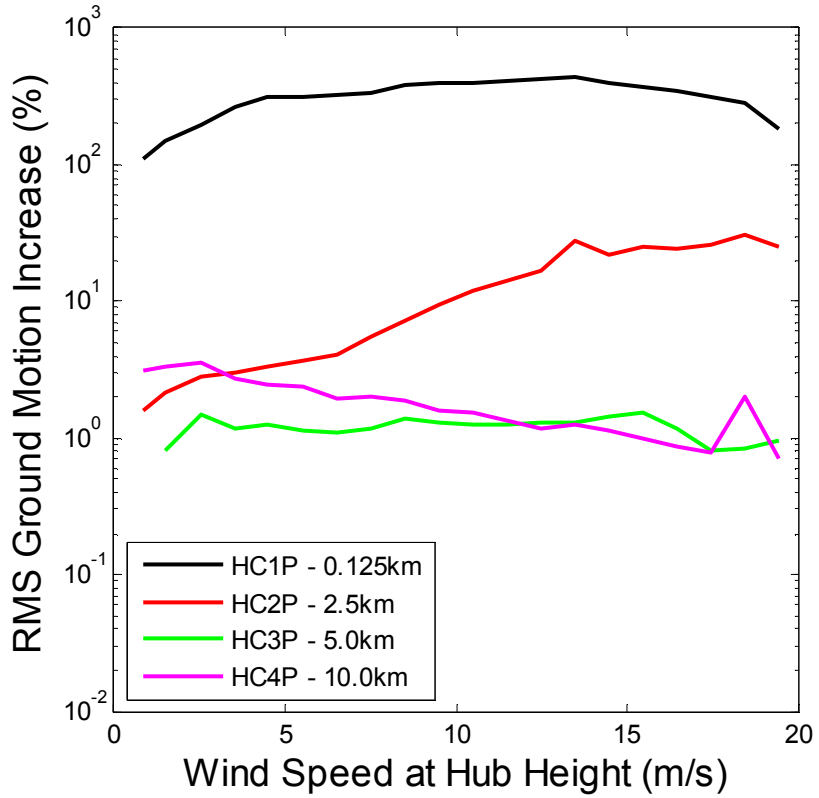
Comparison of RMS background and turbine-influenced values shows that for most stations, the added contribution to the noise due to the presence of the turbines adds only a very minor increase to the ambient background ground motion of between 0.6 − 25% (Fig. 27). The only exception to this is at station HC1P located near the base of turbine #2, where ground motion levels range between approximately 100 − 400% higher than those of the ambient background estimated at HC2P due to the overwhelming influence of structural modes of the turbine tower (Fig. 17). At increasing distances, the turbines' bending, torsional modes and blade-pass harmonics have decreasing influence on the ambient background as the surface waves spread and attenuate. While blade-pass harmonics may increase rapidly with increasing wind speeds between ~8 − 16 m/s, this growth ceases at greater wind speeds by design as the turbine reaches its maximum power output of 3.0 MW (Vestas, 2006). Such behavior is seen at the moderate distance of 2.5 km of station HC2P where influence of the turbines grow from a few percent, but remain steady at an additional ~25% (Fig. 27). At greater distances, such as HC3P (5.0 km), the turbine noise increase is moderated by the increased attenuation by geometrical spreading and results in a nearly constant influence of a few percent. While at even greater distances like that of HC4P (10 km), only the

lowest order turbine tower modes and blade pass harmonics are weakly observed above the ambient background. At this distance, the best observations are during periods of quiet, low background conditions when turbine output and vibration are at a minimum. As winds increase, changes in the ambient background dominate the overall changes in the spectrum, such that even though turbine output and vibration increase, they have an increasingly negligible influence on the overall observed ground motion.

Overall the added, and largely tonal, content of the V-90 turbines' seismic noise behaviour results in only minor amounts of additional noise to the ambient background at kilometre distances. Even at relatively close distances, such as at station HC1P near the base of the turbine, where RMS ground motion increases up to a factor of 4, may be considered moderate and imperceptible by people. The addition of turbine-noise to the background noise at these levels and frequencies, while measureable by sensitive seismographs and a source of undesirable contamination in earthquake monitoring, are not likely to be perceived by local population. To demonstrate this, an example of natural ground shaking is compared to the Summerside Wind Turbine Farm turbine noise.

Wind Speed m/s	HC1P Turbine nm/s	HC2P Bkgrd nm/s	HC2P Turbine nm/s	HC3P Bkgrd nm/s	HC3P Turbine nm/s	HC4P Bkgrd nm/s	HC4P Turbine nm/s
0 − 1	106.77	51.18	51.99	54.95	54.94	53.76	55.44
1 − 2	136.80	54.72	55.91	57.59	58.05	55.64	57.50
2 − 3	188.12	63.12	64.87	65.63	66.59	61.23	63.41
3 − 4	255.89	70.51	72.63	72.06	72.9	67.69	69.56
4 − 5	319.20	77.86	80.46	79.15	80.14	73.35	75.13
5 − 6	333.40	81.53	84.52	81.14	82.05	76.03	77.82
6 − 7	361.84	86.34	89.82	85.11	86.05	80.39	81.96
7 − 8	398.17	91.01	95.97	88.31	89.36	82.81	84.48
8 − 9	457.61	95.87	102.80	92.13	93.39	86.44	88.08
9 − 10	500.27	101.14	110.67	95.11	96.36	90.49	91.95
10 − 11	549.67	111.36	124.46	103.16	104.47	97.54	99.03
11 − 12	618.90	122.27	139.78	111.56	112.97	105.1	106.50
12 − 13	684.18	131.45	153.16	116.9	118.4	110.75	112.06
13 − 14	714.75	134.28	171.67	124.78	126.4	118.32	119.79
14 − 15	770.19	154.00	188.00	131.67	133.58	124.44	125.87
15 − 16	817.77	171.89	214.52	137.73	139.85	132.43	133.73
16 − 17	856.87	194.37	242.26	141.88	143.52	139.96	141.16
17 − 18	904.49	221.66	278.94	153.69	154.95	152.43	153.61
18 − 19	927.65	241.49	315.07	160.77	162.13	157.36	160.47
19 − 20	891.11	315.98	395.27	172.20	173.84	170.23	171.44

Table 15: Computed RMS ground motion amplitudes within the 0.8 − 10 Hz spectral band for the estimated seismic background noise with and without the presence of wind turbine noise.

Fig. 27: Percentage of the added noise contribution by the presence of the Summerside V-90 wind turbines to the ambient seismic background as a function of wind speed for monitoring stations HC1P to HC4P.

5. RMS & Spectral Comparison to Regional Earthquakes

Although the previous section compared the Summerside V-90 wind turbine noise to local ambient seismic background noise levels, it is sometimes difficult to translate what sensitive seismographic instruments are able to measure, to what can be perceived by the average person's experience. While turbine-induced ground motion may be measureable and a source of undesirable noise for sensitive instrumentation (e.g. Schofield, 2001, Styles 2010, Saccorotti et al, 2011), it does not necessarily follow that increases in seismic noise could be perceived during the course of daily life. As shown in the Section 4.3, typical ambient background ground motions are measured at scales of 10's to 100's of nm/s. Thresholds for human perception of vertical vibrational motion lie at ~0.05 − 3.1 m/s between 1 − 10 Hz and ~0.05 − 1.4 m/s for horizontal vibrational motion (Griffin, 1990), thus the typical seismic background lies between 5 − 6 orders of magnitude below that which could be perceived by the average person.

Earthquakes, a natural phenomenon associated with ground shaking, are often used as a comparative by individuals to describe transient or unexpected vibrations, e.g. "It was as if there had been an earthquake". As such it is useful to compare the observed ground motions associated with the Summerside wind turbines to a locally recorded earthquake.

The amount of energy released, and hence the ground motion produced, by an earthquake is highly variable from the very small that would never be perceived without very sensitive instruments, to extremely large that result in significant damage to infrastructure and life. As a result of this wide variability, the scales that is commonly used to measure the overall size or magnitude of an earthquake are base ten logarithmic, such that a magnitude 5.0 earthquake is 10 times more energetic than a magnitude 4.0 and 100 times more than a magnitude 3.0, and so on. In Eastern North America, the specific earthquake magnitude scale most often used is called the Nuttli scale (Nuttli, 1973) and is designated by the abbreviation, m_N, and defined as:

$$m_N = -0.1 + 1.66*\log 10(\ R\ ) + \log 10(\ A/\tau\ ) \qquad \text{for } 50 \text{ km} < R < 3000 \text{ km} \qquad (10)$$

where R is the distance from the earthquake epicenter, A is the ground displacement amplitude in microns (μm), at an observed period, τ, (Nuttli, 1973).

After an earthquake has occurred, the initial energy released in the form of seismic waves spreads outward and becomes subject to attenuation akin to that discussed in Section 4.1. Thus an observer, in general, will experience decreasing amounts of ground motion as their distance from an earthquake increases. As the average person cannot easily determine how their individual experience during ground shaking may translate to the magnitude of an earthquake, an intensity scale called the "Modified Mercalli Intensity Scale" is often used to categorize a person's individual experience. The scale varies from I – XII and is useful in determining how widespread and intense an earthquake's ground motion effects are over a region when reported over large distances. Although the scale is based on individual experiences, if reported over a wide region, it is a useful tool with which to assess the distances that a particular earthquake was felt or perceived.

5.1 The Modified Mercalli (MM) Intensity Scale

The Modified Mercalli intensity scale is designed to describe the effects of the ground shaking caused by an earthquake, as experienced at a given place, on natural features, urban and industrial installations and upon human beings. The intensity of an earthquake differs from the earthquake magnitude. Earthquake magnitude is related to the energy released by an earthquake, while its intensity is related to the effects the release of this energy has on infrastructure and people over an area or region. There are multiple versions of the MM scale; the one described here is the Wood and Neumann (1931) version (Table 16).

Table 16: The modified Mercalli scale of earthquake intensity

Intensity Scale Level	Shaking	Damage	Description
I	Not Felt	None	Felt only under especially favourable circumstances. Under certain conditions, sometimes birds, animals are reported uneasy or disturbed; sometimes dizziness or nausea experienced; sometimes trees, structures, liquids, bodies of water, may sway - doors may swing, very slowly.
II	Weak	None	Felt indoors by few, especially on upper floors, or by sensitive, or nervous persons. Also, as in grade I, but often more noticeably: sometimes hanging objects may swing; trees, structures, liquids, bodies of water, may sway, doors may swing, very slowly; sometimes birds, animals, reported uneasy or disturbed; sometimes dizziness or nausea experienced.
III	Weak	None	Felt indoors by several, motion usually rapid vibration. Sometimes not recognized to be an earthquake at first, duration estimated in some cases. Vibration like that due to passing of light, or lightly loaded trucks, or heavy trucks some distance away. Hanging objects may swing slightly. Movement may be appreciable on upper levels of tall structures. Standing cars may rock slightly.
IV	Light	None	Felt indoors by many, outdoors by few. Awakens few, especially light sleepers. Frightens no one, unless apprehensive from previous experience. Vibrations like that due to passing of heavy, or heavily loaded trucks. Sensations like heavy body striking building, or falling of heavy objects. Rattles dishes, windows, doors; glassware and crockery clink and clash. Creaking of walls, framing. Hanging objects swing, in numerous instances. Disturbs liquids in open vessels slightly. Standing cars may rock slightly.
V	Moderate	Very Light	Felt indoors by practically all, outdoors by many or most. Outdoors direction may be estimated. Awakened many, or most. Frightens few - slight excitement, few may run outdoors. Buildings tremble throughout. Broken dishes, glassware, to some extent. Cracks windows in some cases, but not generally. Overturns small or unstable objects, in many instances, with occasional fall. Hanging objects, doors, swing generally. Knocks pictures against walls, or swung out of place. Opens or closes doors, shutters abruptly. Moves small objects, furnishings, the latter to slight extent. Spills liquids in small amounts from well-filled open containers. Trees, bushes, shake slightly.
VI	Strong	Light	Felt by all, indoors and outdoors. Frightens many, excitement general, some alarm, many run outdoors. Awakens all. Persons made to move unsteadily. Trees, bushes, shaken slightly to moderately. Liquid set in strong motion. Small bells ring; church, chapel, school etc. Damage slight in poorly built buildings. Fall of plaster in small amount. Cracks plaster somewhat, especially fine cracks, in some instances also in chimneys. Brakes dishes, glassware, in considerable quantity, also some windows. Fall of knick-knacks, books, pictures. Overturned furniture, in many instances. Moved furnishings of moderately heavy kind.
VII	Very Strong	Moderate	Frightens all - general alarm, all run outdoors. Some, or many, find it difficult to stand. Noticed by persons driving cars. Trees and bushes shaken moderately to strongly. Waves on ponds, lakes, and running water. Water is turbid from stirred up mud. Collapse to some extent of sand or gravel stream banks. Rings large church bells, etc. Suspended objects made to quiver. Damage is negligible in buildings of good design and construction, slight to moderate in well-built ordinary buildings, considerable in poorly built or badly designed buildings, old walls (especially when laid without mortar), spires, etc. Cracks chimneys to considerable extent, walls to some extent. Fall of plaster in considerable to large amount. Brakes numerous windows, furniture to some extent. Shakes down loosened brickwork and tiles. Brakes weak chimneys at the roof-line. Fall of cornices from towers and high buildings. Dislodged bricks and stones. Overturns heavy furniture, with damage from breaking. Considerable damage to concrete irrigation ditches.

VIII	Severe	Moderate – Heavy	Fright general - alarm approaches panic. Disturbs persons driving cars. Trees shaken strongly - branches, trunks, broken off, especially palm trees. Ejects sand and mud in small amounts. Changes either temporarily or permanently; in flow of springs and wells; dry wells renewed flow; in temperature of spring and well waters. Damage slight in structures (brick) built especially to withstand earthquakes. Considerable in ordinary substantial buildings, partial collapse of wooden houses in some cases; Dislodging of panel walls in frame structures, brakes off decayed pilings. Fall of walls. Cracked, broken, solid stone walls seriously. Wet ground to some extent. Twisting, fall, of chimneys, columns, monuments, factory stack, towers. Moves conspicuously, overturns, very heavy furniture.
IX	Violent	Heavy	Panic general. Cracks ground conspicuously. Damage is considerable in (masonry) structures built especially to withstand earthquakes: throws out of plumb some wood-frame houses built especially to withstand earthquakes. Damage is great in substantial (masonry) buildings, with some collapse. Frame buildings wholly shifted off foundations, racked frames. Serious damage to reservoirs; underground pipes sometimes broken.
X	Extreme	Very Heavy	Panic general. Cracks ground, especially when loose and wet, up to widths of several inches. Fissures run parallel to canal and stream banks. Landslides considerable from river banks and steep coasts. Shifts sand and mud horizontally on beaches and flat land. Changes level of water in wells. Throws water on banks of canals, lakes, rivers, etc. Damage is serious to dams, dikes, embankments. Severe to well-built wooden structures and bridges, some destroyed. Development of dangerous cracks in excellent brick walls. Destroys most masonry and frame structures, also their foundations. Bends railroad rails slightly. Buried pipelines torn apart, or crushed endwise. Opens cracks and broad wavy folds in cement pavements and asphalt road surfaces.
XI	Very Extreme	Severe	Panic general. Disturbances in ground are many and widespread, varying with ground material. Broad fissures, earth slumps, and land slips in soft, wet ground. Ejects water in large amounts charged with sand and mud. Causes tsunamis of significant magnitude. Damage is severe to wood-frame structures, especially near shock centers. Great damage to dams, dikes, embankments, often for long distances. Few, if any, masonry structures remain standing. Destroys large well-built bridges by the wrecking of supporting piers, or pillars. Affects yielding wooden bridges less. Bends railroad rails greatly, and thrusts them endwise. Puts pipe lines buried in earth completely out of service.
XII	Beyond Extreme	Total Destruction	Panic general. Damage total - practically all works of construction damaged greatly or destroyed. Disturbances in ground are great and varied, numerous shearing cracks. Significant landslides, rock falls, slumping of river banks, etc. numerous and extensive. Wrenched loose, tore off, large rock masses. Fault slips in firm rock, with notable horizontal and vertical offset displacements. Water channels, surface and underground, disturbed and modified greatly. Dams lakes, produces waterfalls, deflects rivers, etc. Waves seen on ground surfaces (actually seen, probably, in some cases). Distorted lines of sight and level. Objects thrown upward into the air.

Table 16 (cont'd): The modified Mercalli scale of earthquake intensity.
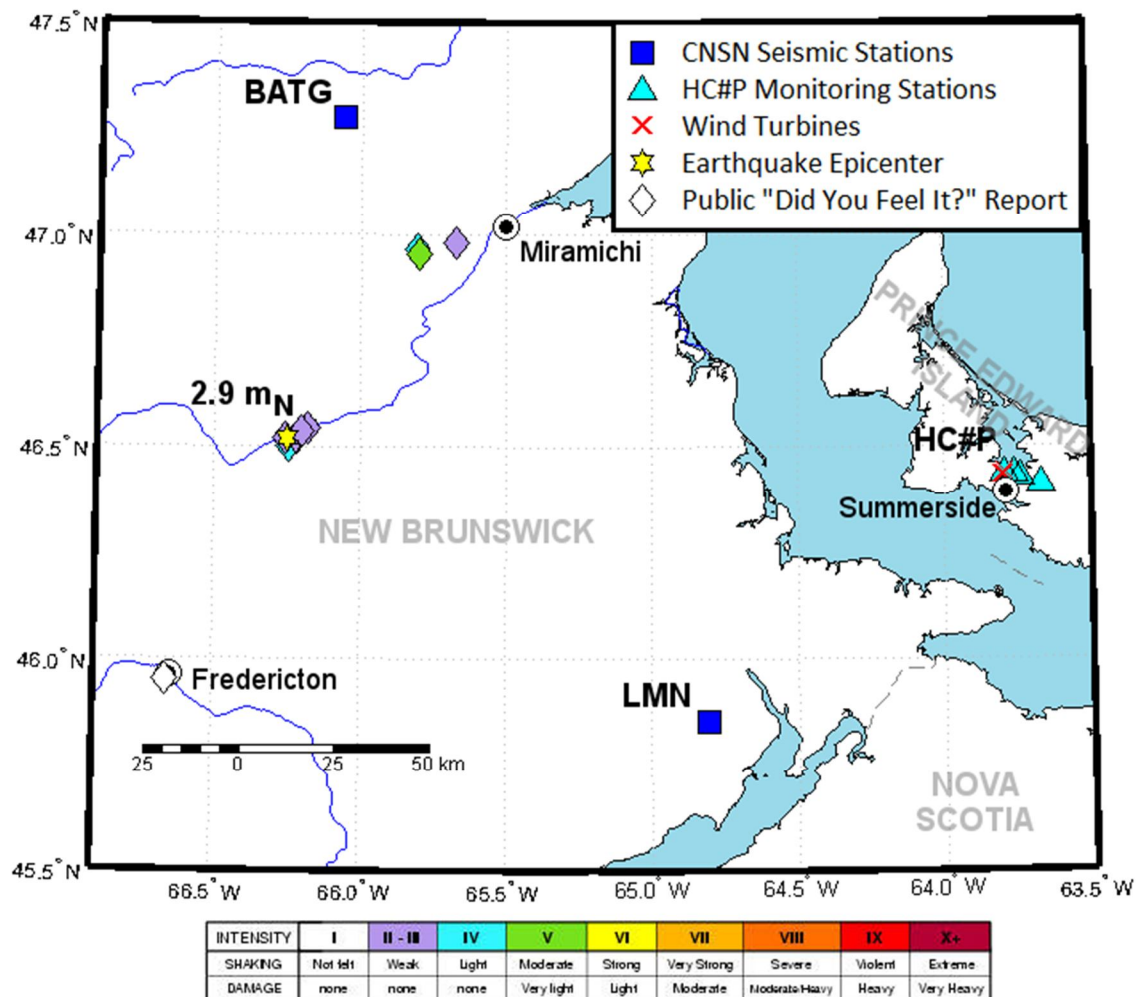
5.2 June 20, 2013 Magnitude 2.9 Earthquake

On the 20th of June, 2013 a shallow earthquake was recorded by the Canadian National Seismic Network (CNSN) and located by *EarthquakesCanada* as having occurred midway between Mirimichi and Fredericton, New Brunswick, near the village of Carrolls Crossing at 01:37:20 UTC (or 05:37:20 EDT) with an epicenter at 46.5196°N 66.2489°W and at an estimated depth of 5.0km (Fig. 28). The earthquake was observed by more than 25 regional seismic stations throughout New Brunswick, Quebec, The Maritimes and Maine, including the wind turbine monitoring stations near Summerside, PEI, with a reported magnitude of 2.9 ± 0.1 m_N. This event is unique during the monitoring period as the only earthquake in the region reported as "felt" by the public and observed by the HC#P stations.
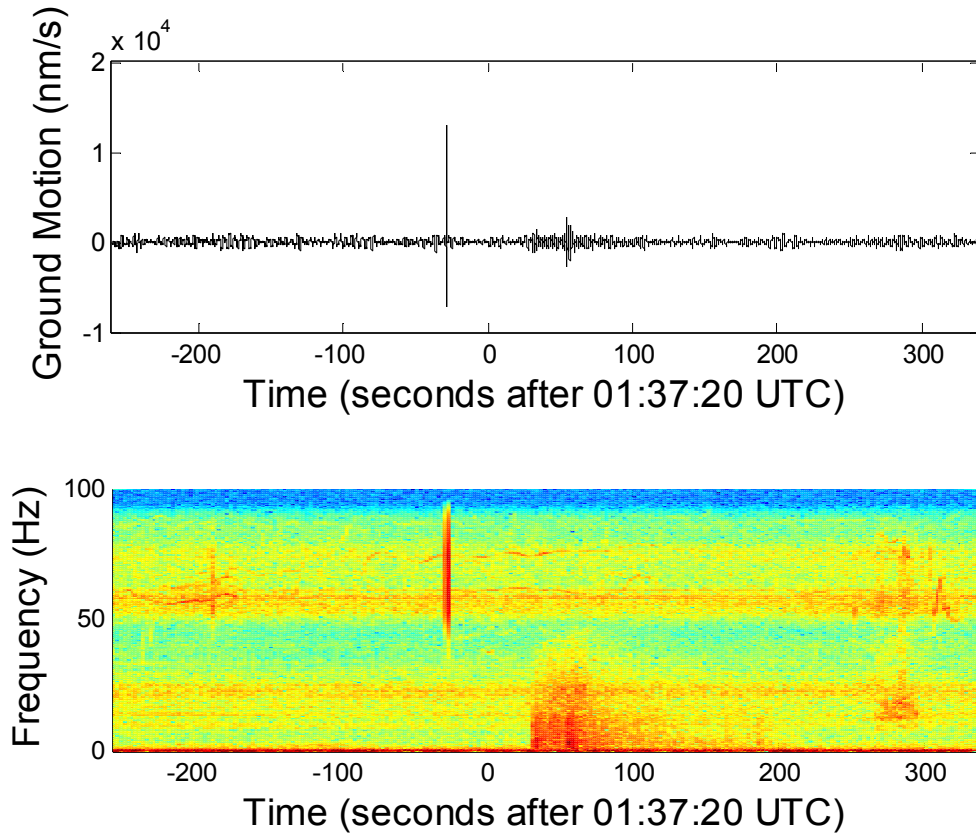
Soon after the earthquake, reports by the public were reported to *EarthquakesCanada* through its online "Did you feel it?" (DYFI) reporting page (http://www.earthquakescanada.nrcan.gc.ca/dyfi-lavr/known-connu-eng.php). A total of 10 DYFI reports were received for this earthquake reporting weak to moderate shaking mostly in the region surrounding the earthquake's epicenter to a distance of 67.5 km from the epicenter (Fig. 28). Although instruments were not present near the epicenter, CNSN stations BATG and LMN are located at comparable distances to the furthest reports of felt shaking and the PEI monitoring stations at 82 and 135 km, respectively. These provide a measure of comparison to observations of the same earthquake recorded by the monitoring stations in PEI at a distance range of 190 – 200 km.

Observations of the June 20, 2013 earthquake were recorded on the PEI monitoring stations during a period of calm winds between 1.4 – 3.0 m/s, when turbine-related seismic noise levels were near their minimum (Fig. 17 – 20). Spectrograms and time domain waveforms for the monitoring stations show the arrival at 01:37:49.8 UTC (05:37:49.8 EDT) of the earthquake's primary (P or compressive) waves and ~23 seconds later secondary (S or shear) waves within the 0.8 – 30 Hz frequency band, alongside a spectrum punctuated by bands of tonal noise from nearby anthropogenic sources (Fig. 29). If the raw data is filtered within this passband, a clearer view of the earthquake signal is seen (Fig. 30) as it reaches peak ground motions of 2830 nm/s. Similar waveforms are seen arriving at HC2P, HC3P and HC4P at progressively later times with increasingly smaller amplitudes to a motion of 1440 nm/s at HC4P.
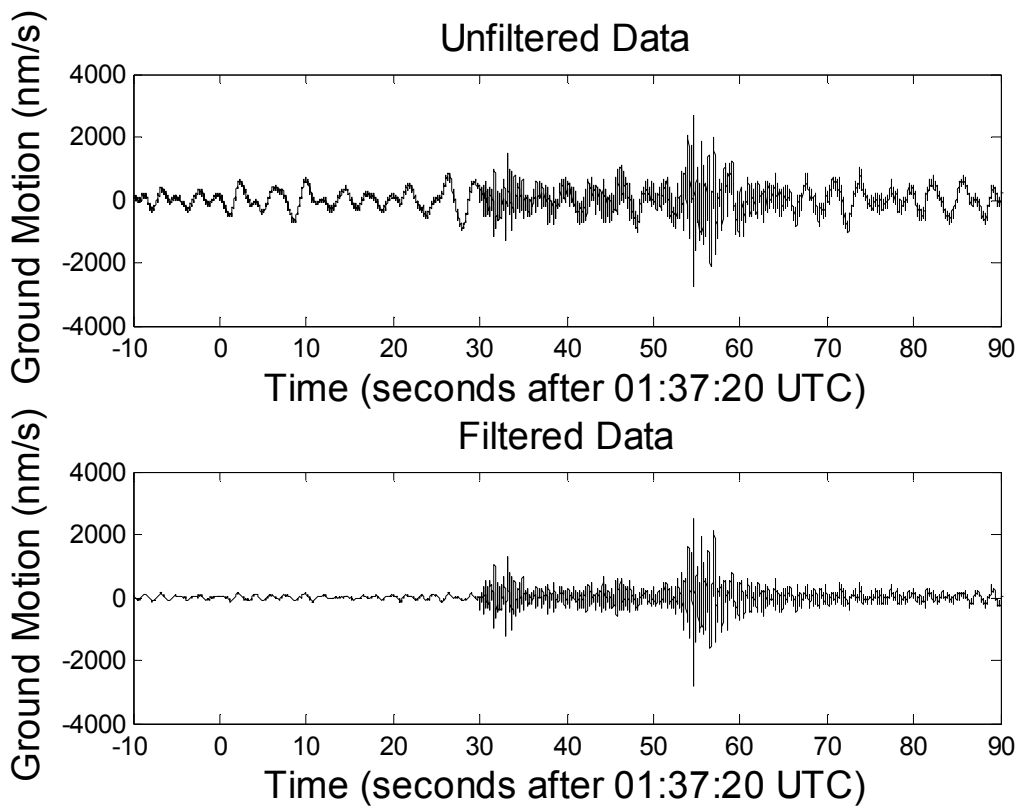
No testimonies to experiencing the effects of ground shaking were reported to *EarthquakesCanada* in PEI for this event. Similarly, at CNSN station LMN where ground motions were comparable in amplitude to that in PEI (Fig. 31), no reports of felt shaking were received. At CNSN station BATG, ground motions reached a peak of more than twice that observed by the HC#P stations (Fig. 32). It is only after reaching ~20 km closer to the earthquake epicenter than station BATG, towards the town of Miramichi, NB that the first felt reports of weak to moderate shaking (MMII – V) are reported (Fig. 28). At this distance (57 – 66 km from the epicenter) ground shaking was likely still greater than that recorded by BATG.
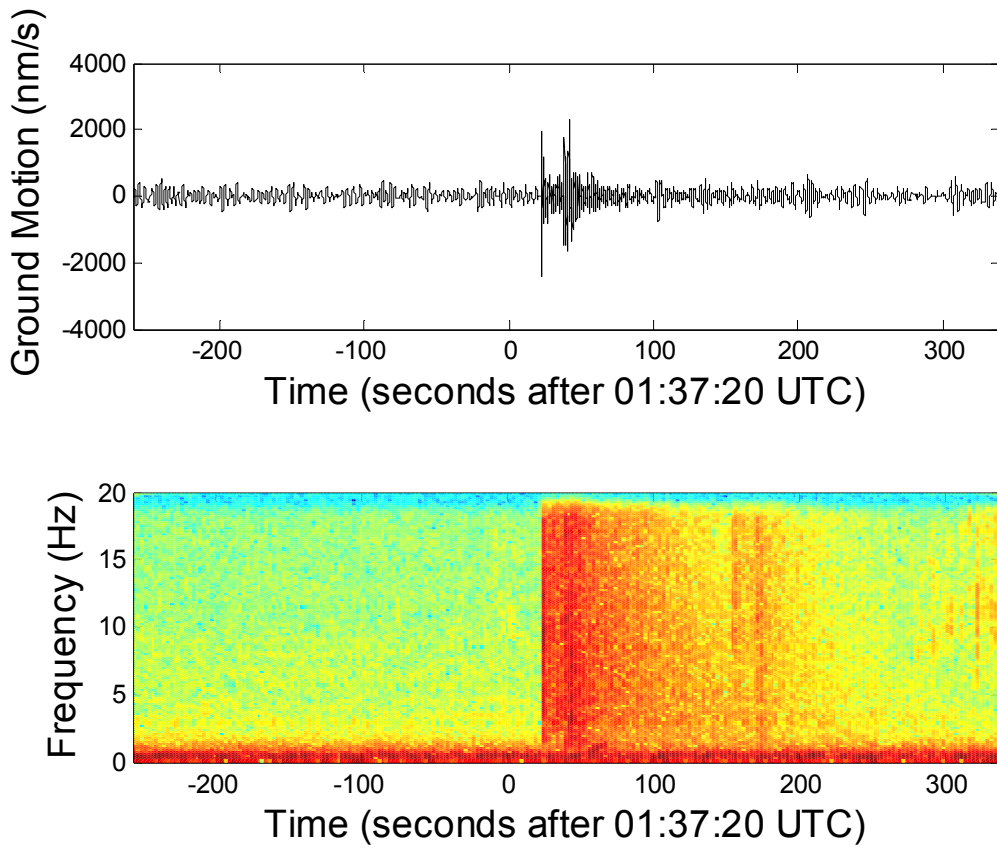
Fig. 28: Regional map of the magnitude 2.9 m_N earthquake in New Brunswick on June 20, 2013. Public reports of felt shaking are shown as coloured diamonds, white diamonds indicate reports of no shaking felt. Colours indicate the level of experienced shaking on the Modified Mercalli Intensity Scale. Nearest reporting seismic stations BATG (82 km distant from epicenter) and LMN (135 km distant) are shown relative to the monitoring stations HC1P – HC4P (190 – 200 km distant) near Summerside, PEI.
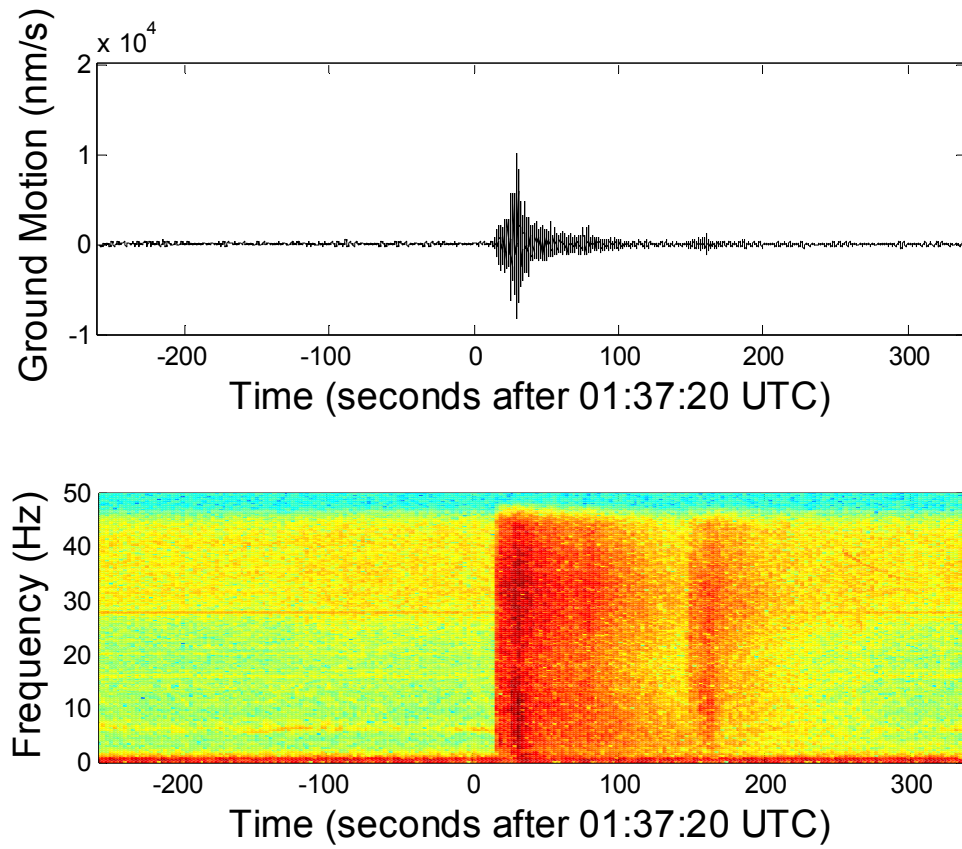
Fig. 29: Arrival of seismic waves at HC1P from the magnitude 2.9 m_N earthquake on June 20, 2013 in New Brunswick (above), as measured in ground motion at an epicentral distance of ~190 km. The same period of time as seen by spectrogram (below), shows frequency content of these arrivals between 30 – 150 seconds and 0.8 – 30 Hz. Background noise at time shows bands of largely tonal noise from local anthropogenic sources and a single high frequency spike at approximately -20 seconds.
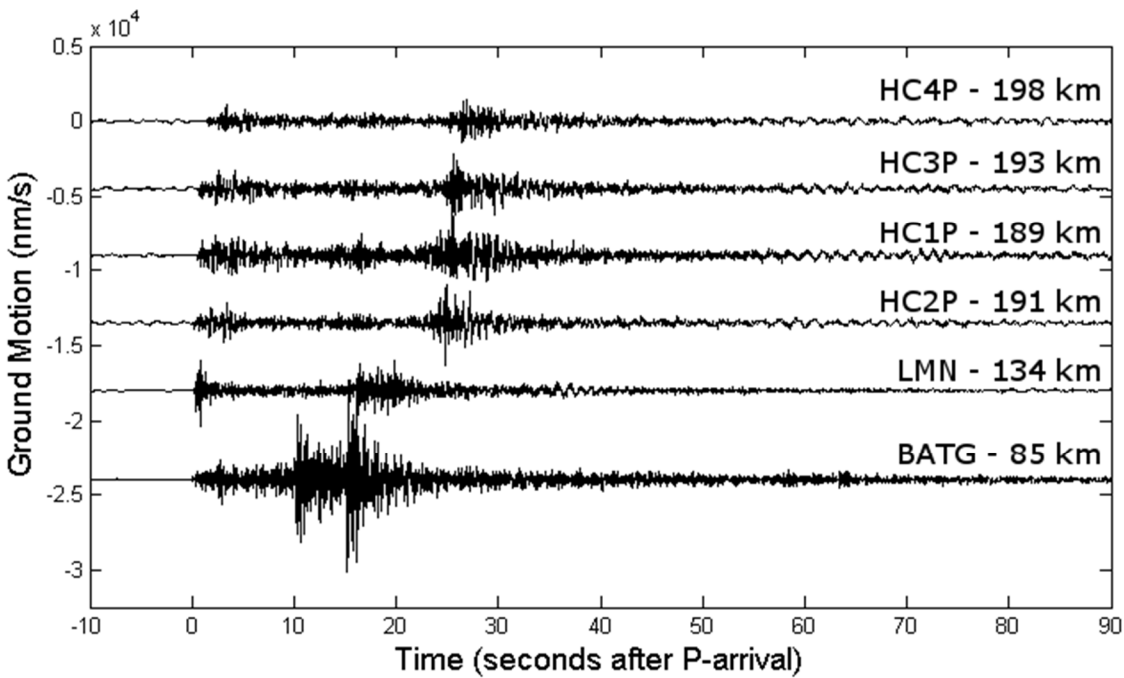
Fig. 30: Example of the raw unfiltered ground motion data for station HC1P (above) and bandpass filtered between 0.8 – 30 Hz (below) at a distance of 190 km from the June 30, 2013 New Brunswick 2.9 m_N earthquake. Similar observations are also seen at stations HC2P, HC3P and HC4P with decreasing strength with increasing distance. Peak ground motions are associated with the secondary or S-wave arrivals and reached 2830 nm/s at HC1P, 2640 nm/s at HC2P, 2350 nm/s at HC3P and 1440 nm/s at HC4P.

Fig. 31: Arrival of seismic waves at CNSN station LMN near Caledonia Mountain, NB from the magnitude 2.9 m_N earthquake on June 20, 2013 in New Brunswick (above). The same period of time as seen by spectrogram (below). At a range of 135 km, arrivals at LMN show earthquake-related frequency content from ~1 Hz up to the Nyquist frequency of ~18 Hz, comparable to that seen at HC1P (Fig. 30). The second set of arrivals at ~150 seconds associated the earthquake's aftershock are also visible. Peak ground motion seen at LMN reached 2390 nm/s.
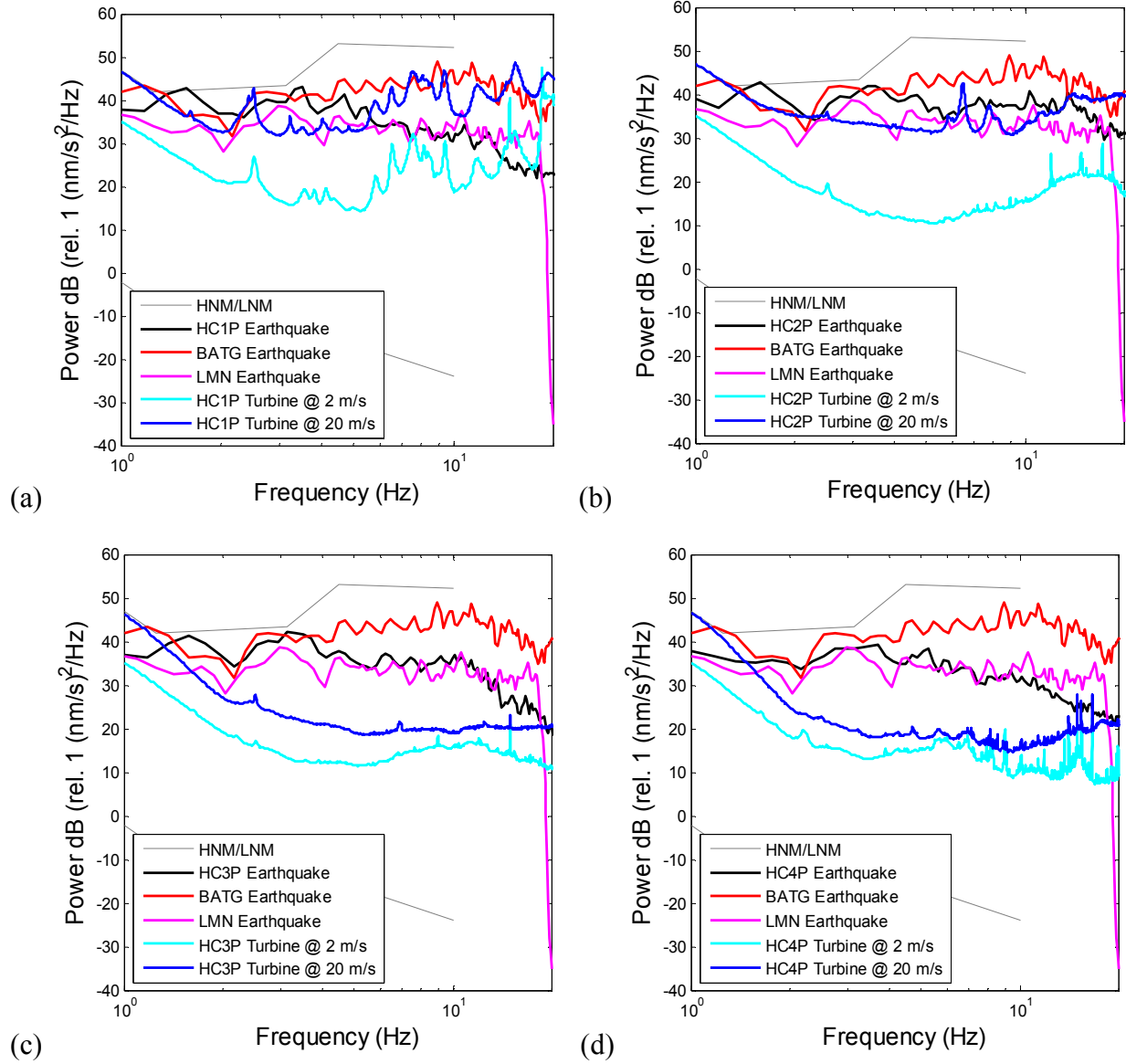
Fig. 32: Arrival of seismic waves at CNSN station BATG near Bathurst, NB from the magnitude 2.9 m$_N$ earthquake on June 20, 2013 in New Brunswick (above). The same period of time as seen by spectrogram (below). At a range of 82 km, arrivals at BATG show significant energy at frequencies content from 0.8 Hz up to the Nyquist frequency of ~46 Hz. A second set of arrivals can be seen at ~140 seconds associated with an aftershock of the earthquake, not seen at station HC1P and only weakly at LMN. Peak ground motion at BATG reached 6650 nm/s.

Fig. 33: Comparison of waveforms and relative ground motion observed from 85 to ~200 km from the epicenter of the June 20, 2013 magnitude 2.9 mN earthquake in New Brunswick. Amount of ground shaking observed at 85 km is 2.3 – 4.6 times greater than that observed by the monitoring stations in PEI.

If ground motions due to the June 20, 2013 earthquake observed from the PEI monitoring stations are compared with estimates of the increased seismic background motions due to the Summerside V-90 wind turbines (Table 14), it is observed that the turbine-related noise is a factor of between 1.5 to 50 times smaller than the motion recorded by any of these stations during the earthquake's signal (Fig. 33). This contrast in motion between the Summerside turbines and the earthquake is also observed when comparing spectra from both the earthquake and turbine-related ground motions (Fig. 34). Here even turbine-related ground motion spectra during high winds (20 m/s) lie typically between 5 and 20 dB below much of the earthquake spectrum observed at the same station, translating to amplitudes that are factors of 2 to 10 times smaller at these frequencies.

Overall, as the earthquake shaking experienced in PEI on June 20, 2013 was itself at least a factor of 2 to 4 times smaller than the apparent threshold of human perception according to public DYFI reports (Fig. 28) and ground motion observations at BATG (Figs. 32, 33), it is highly unlikely that the additional ground motion that is induced by the vibration of the four Summerside V-90 wind turbines would be perceptible by a person at the distances measured during this study, even during the highest of wind conditions.
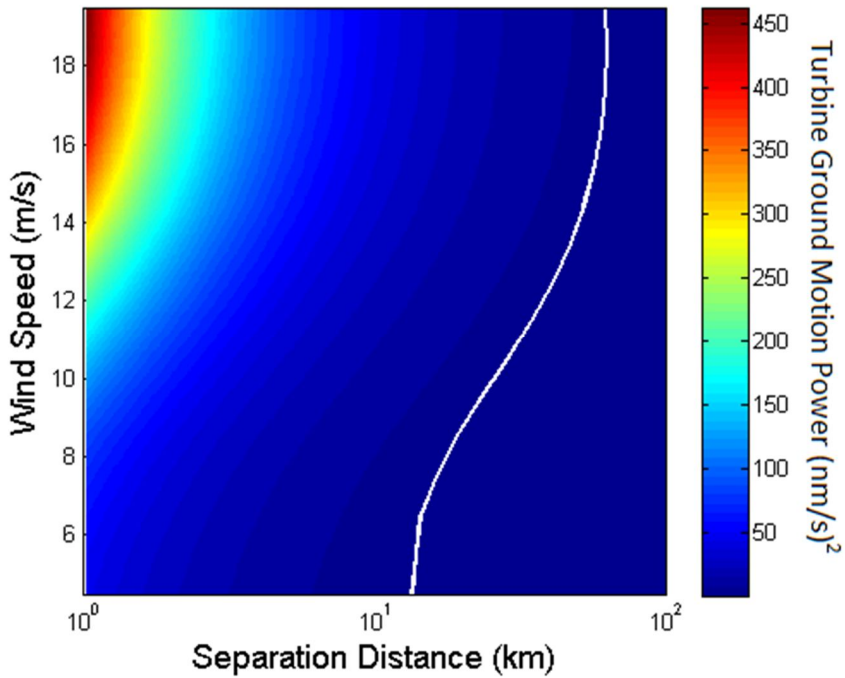
Fig. 34: Power Spectral Density comparison of the ground motion arrivals recorded by the PEI seismo-acoustic monitoring and CNSN stations of the June 20, 2013 magnitude 2.9 m_N earthquake, and the inner-quartile mean ground motion associated with the Summerside wind turbines during both low and high wind conditions at; HC1P (a) HC2P (b) HC3P (c) HC4P (d). In nearly all cases wind turbine-related spectral noise lies significantly below that of the earthquake, and well below that of station BATG, closest to reports of the earthquakes being felt.

6. Turbine Noise Contamination to Seismic Monitoring Stations

In Canada, an increasing desire to move to renewable energy sources for electrical power generation, has resulted in the total installed capacity in wind energy to rise in Canada from 7,803 MW in 2013 to 9,219 MW in 2014 for an overall ~18% increase. (Canadian Wind Energy Association, 2014). The rise in numbers of wind turbines and wind turbine facilities means that increasingly a number of permanent seismic monitoring stations of the Canadian National Seismic Network (CNSN) are being encroached upon by wind turbines. As has been seen in the case of the Summerside, PEI turbines, the presence and operation of wind turbines can be readily observed in data gathered by sensitive seismometers. This is a new source of undesirable noise within the ~0.5 – 10 Hz monitoring band for regional earthquakes and few policies exist for the planning of wind turbine construction to allow mutual co-existence of both technologies. If this is to occur, the question of "What separation distance is necessary to prevent undesirable noise on a seismometer by one or more wind turbines", must be answered. The Summerside wind turbine noise study is a first step towards answering this question.

Using the observations of the four Vestas 3.0MW V-90 turbines at multiple separation distances, a model of the growth and attenuation of the turbines' far field noise was constructed (Section 4). In addition, measurements of the changes in ambient background seismic noise with increasing wind speeds were also documented (Section 5). Together these two models can be used to determine what separation would be necessary to install a permanent seismic station from a wind energy facility such as Summerside without observing the seismic noise generated by the facility. A minimum necessary separation can be defined as the distance at which the lowest observable harmonic of both the blade pass frequency and tower are equal to the level of the ambient seismic background. In the specific case of the Summerside wind turbine facility, this would be the peaks associated with the 3BP and 2BM, centered at 2.41 and 2.50 Hz respectively. The lowest order harmonics are used, as these frequencies both lie within the regional monitoring frequency band, are the most energetic of all the observed harmonics and experience the least amount of attenuation of all observed harmonics and so are most likely to be observed at large distances.

Evaluating and equating the seismic spectral growth and attenuation models for harmonic modes 3BP and 2BP (Sections 4.0 and 4.2), with the mean ambient noise level models for monitoring stations HC2P, HC3P and HC4P (Section 4.3, Equation 9, Tables 11-13) within the 3BP/2BM frequency band (2.37 – 2.58 Hz), provides an estimate of the minimum separation distance. The procedure is repeated for each measured wind speed bin to map the minimum separation distance as a function of wind speed (Fig. 35). When evaluated, it is observed that at low wind speeds a separation distance of 13.5 km is required when both the turbines and the ambient noise are at low levels. This minimum separation quickly grows with increasing wind speed, as turbine noise grows more rapidly than the ambient background, to a peak of 62.6 km at 18.5 m/s. At this point growth of the turbine noise tapers off as the 3BP/2BM harmonics reach their peak levels (Fig. 35). Should the ambient levels continue to grow further with increasing wind speed, while turbine noise remains steady, the minimum separation distance would begin to decrease. From this comparison any separation greater than ~63 km would be sufficient to prevent observation of the Summerside wind turbine facility by a permanent seismic monitoring facility.

Fig. 35: Model of the growth and attenuation of the 2BM/3BP seismic noise resulting from the four Summerside Vestas 3.0MW V-90 turbines as a function of wind speed and distance. The minimum separation distance for a hypothetical seismic monitoring station to not observe the facility noise is shown as a white curve.

This procedure of determining a minimum separation is dependent upon the consistent behaviour of the ambient background regardless of location. The separation could be substantially different if changes in the ambient background with wind speed were more marginal. This might be the case for a monitoring station to be located on local bedrock, as opposed to soil (e.g. Bowers, 2013). As well, since the facility's noise output scales with the number of turbines and harmonics are dependent upon the physical properties of those turbines, the procedure of determining appropriate separation distances can quickly become facility, region and/or site dependent.

6.1 Wind Speed Probability and Turbine-Instrument Separation
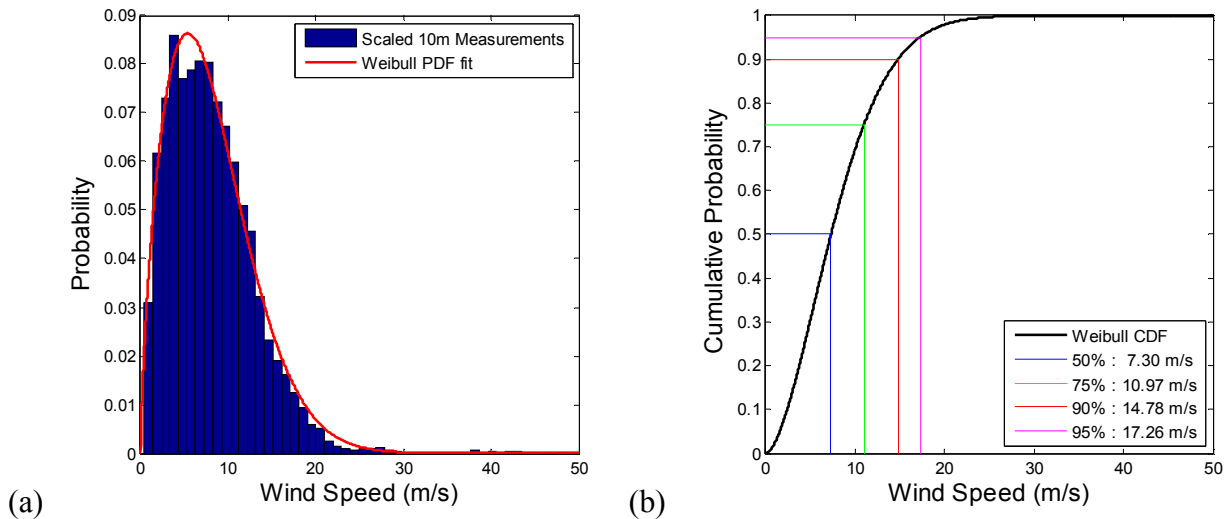
Other considerations can also become concerns as available/appropriate sites for locating a monitoring station are constrained by other factors. For instance, the number of possible locations greater than 63 km from the Summerside facility and appropriate for seismic monitoring would be constrained by the physical size of the island itself, locations of urban infrastructure and other sources of undesirable anthropogenic seismic noise. In this way, it may not be possible to locate a site at the extreme separation limits, in such cases it is still desirable to seek to minimize exposure to a turbine facility's noise.

A turbine facility's seismic noise output is dependent upon the wind conditions it is exposed to. While a facility may be designed for maximum output for the wind conditions of a region, such wind conditions are not always present. The probability of a particular wind speed present at a location is commonly described by the Weibull probability distribution (Justus et al., 1976):
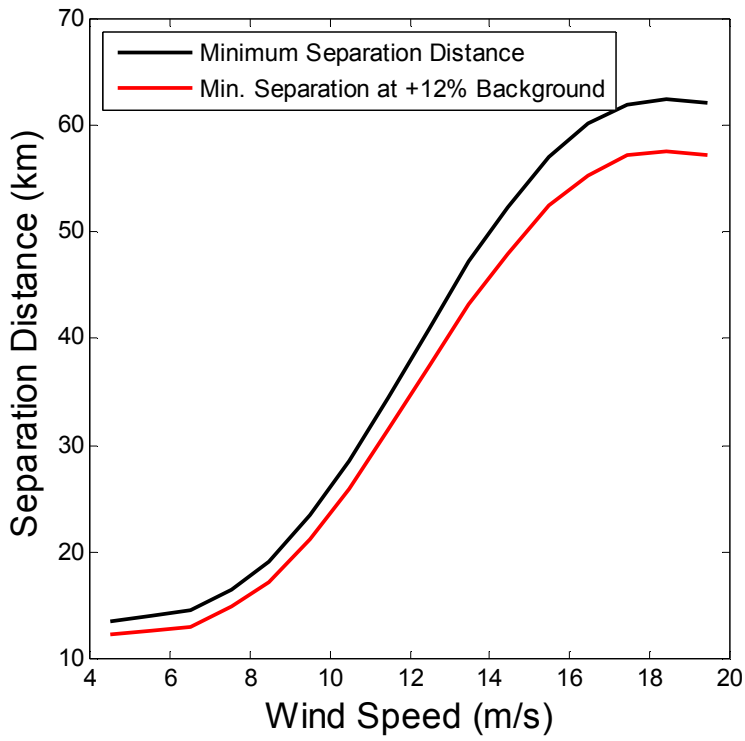
$$f(w; \lambda, k) = \begin{cases} \frac{k}{\lambda} \left(\frac{w}{\lambda}\right)^{k-1} e^{-(w/\lambda)^k} & w \geq 0 \\ 0 & w < 0 \end{cases} \tag{11}$$

where k is the shape parameter, λ is the scaling parameter, and w is the wind speed. If the parameters k and λ are fitted to the scaled observations made for the Summerside wind turbine facility (Section 3), values of $\lambda = 9.05 \pm 0.06$ and $k = 1.70 \pm 0.01$ are determined via maximum likelihood (Seguro and Lambert, 2000). The Weibull distribution fits the wind speed observations quite well (Fig. 36a), and results in a distribution which is skewed to lower wind speeds and displays a long tail towards higher winds.

Using the Weibull cumulative distribution (Fig. 36b), the median of the distribution (or 50th percentile) is found to occur at 7.3 m/s with a 90th percentile occurring at 14.8 m/s. Placing these wind speed probabilities in terms of separation distance, this indicates that a station located 16 km from the facility should expect to observe turbine noise in 50% of its data, while at a 31.5 km separation it would avoid 75% of the turbine noise and 90% of noise at 53.8 km. Alternatively, separation distance might also be reduced if certain levels of turbine noise are agreeable, for instance allowing even a +1 dB level of turbine fundamental noise over background levels (~12% increase) would reduce the minimum separation at all wind speeds from 13.5 km at 4.5 m/s to 12.1 km and 62.6 km at 18.5 m/s to 57.7 km (Fig. 37). A combination of these two methods might also provide grounds for discussion in instances where turbine facilities are significantly large and/or available space is very limited.


(a)   (b)

Fig. 36: (a) Histogram of measurements of wind speed at 10 m height scaled to the hub height of 80 m for the Summerside V-90 turbines. Red curve is the resulting maximum likelihood least squares fit of these measurements to the Weibull probability distribution function. (b) Cumulative distribution function for the fitted Weibull distribution and positions of the 50th, 75th, 90th and 95th percentiles.

Fig. 37: Minimum separation distance for a seismic monitoring station from the Summerside Wind Turbine Facility to avoid turbine noise, as a function of wind speed (black line). An alternative separation distance function (red line), allows a +1 dB in ground motion power (a ~12% increase) for turbine noise over the background.

7. Analysis Summary

From May 5, 2013 to May 22, 2014, NRCan and HC participated in a joint monitoring project to simultaneously record the infrasound and seismic noise of a modern mega-watt class wind turbine farm under normal operating conditions. The study was carried out in the region surrounding the Summerside Wind Farm north of Summerside, PEI and involved continuous monitoring of four seismo-acoustic stations at distances ranging from 125m to 10 km from four Vestas 3.0MW V-90 wind turbines, and meteorological data collection. Analysis of the resulting seismic data from this study has been used to identify in the near and far fields the seismic noise generated by these turbines, and model the growth and attenuation of this noise in the far field. These observations and models are then used to provide estimates of the likelihood of area residents perceiving the seismic vibrations and a means of computing the physical separation required to prevent the recording of turbine noise by a hypothetical seismograph station.

Seismic noise characteristics of the Vestas 3.0MW V-90 turbines are characterized by multiple vibrational and possibly torsional modes related to the sway and flexure of the 80 m turbine tower, along with multiple harmonics related to the passing of the turbine blades in front of the tower. These observations are consistent with similar studies performed with various other types of wind turbines by Schofield (2002), Styles et al. (2005), Styles (2010), Saccorotti et al. (2011), and Bowers (2013). In the near field close to the turbines, seismic noise is dominated by tower

vibrational modes at frequencies > ~1 Hz. This is likely due to the proximity of the station to the turbine tower where vibrational motions of the turbine are coupled to the surface through its foundation. In the far field, the turbine noise is characterized by the presence of the turbine tower's second order bending mode (2BM) at ~2.50 Hz and multiple harmonics of the blade pass frequency (3 - 4BP) with frequencies consistent with the maximum 16.1 RPM rotation rate of the 3.0 MW V-90 turbines, with spectral growth with increasing wind speed, consistent with published operating specifications for these turbines (Vestas, 2006). Attenuation of these seismic vibrations is consistent with transmission primarily through the local sandstone bedrock as surface waves with minimal anelastic attenuation.

Observations of a magnitude 2.9 m_N regional earthquake in New Brunswick on June 20, 2013 by the turbine monitoring stations are used to compare with turbine noise estimates to assess the likelihood of area residents perceiving wind turbine seismic noise. Comparison of data show that even during peak output of the V-90 turbines, the seismic noise generated is less than that of the distant earthquake (except at the nearest station HC1P where peak turbine noise is comparable). As no DYFI reports were received at the time by area residents of the more energetic earthquake, it is unlikely that seismic noise generated by the turbines would be perceived by area residents.

Models of the growth and attenuation of the Summerside V-90 turbines were used to determine the minimum separation required for the turbine noise to not be recorded by a hypothetical seismograph station in the area by equating the most energetic 3BP and 2BM modes to that of the ambient background. For the four Vestas 3.0MW V-90 turbines of the Summerside facility this separation varies between 13.5 – 62.6 km between the measured 4.5 and 19.5 m/s wind speeds. Placement of a station at closer distances than this physical separation could be achieved if tolerances were given to either allow limits on the amount of turbine noise observed, or agreeable limits were placed upon the number of hours that turbine noise would be visible, or a combination of both. These approaches may be useful either in the planning stages of a turbine facility near an existing seismograph site, the installation of a seismic monitoring station near an existing turbine facility, or at an existing seismograph monitoring site which is experiencing undesirable levels of noise but is able to be re-located.

An alternative approach to wind turbine and seismic monitoring "co-existence" is that of determining a "noise budget" such as that proposed discussed by Bowers (2013) and (Xi Engineering Consultants Ltd, 2014) for the International Monitoring Network array EKA in Eskdalemuir, Scotland. In this method, a limit is placed upon the total cumulative amount of noise that all turbine facilities may generate near a station. The amount of noise that would be generated by a facility is then evaluated using a normalized spectrum of the proposed turbine's far field noise characteristics and scaled by both distance from the array and frequency band of interest.

In all the mitigation methods discussed, knowledge of a region's geologic properties, local ambient seismic noise and the specific turbine model's seismic noise characteristics are required, all as a function of wind speed, to properly evaluate and assess how both station and turbine facilities may interact. This will require periods of data collection and assessment, coordination and cooperation between both seismic monitoring and wind turbine operators, with trust that the needs and requirements of both parties will be respected and strived towards.

Acknowledgements

References

AMEC Earth and Environmental, 2009. Preliminary Geotechnical Investigation: Proposed Wind Turbine Number 4, Summerside Prince Edward Island, Geotechnical Report: TE51100, January 2009, 116 pgs.

Bowers D., 2013. Initial study of seismic ground vibration data from mega-watt class turbines, Eskdalemuir Working Group Interim Report. 65 pgs.

Bowman J.R., G. E. Baker, and M. Bahavar, 2005. Ambient infrasonic noise, Geophysical Research Letters, 32, L09803, doi:10.1029/2005GL022486.

Campbell K.W., 2009. Estimates of Shear-Wave Q and k_o for Unconsolidated and Semiconsolidated Sediments in Eastern North America, Bulletin of the Seismological Society of America, 99 (4), 2365-2392, doi: 10.1785/0120080116.

Canadian Wind Energy Association, 2014. CanWea: Installed Capacity. http://canwea.ca/wind-energy/installed-capacity/, (Last Accessed: December 2014).

Environment Canada, 2008. Canadian Wind Energy Atlas. http://www.windatlas.ca/en/index.php (last accessed: December 2014).

Federation of Digital Seismographic Networks, 2012. Standard for the Exchange of Earthquake Data (SEED) Reference Manual, Version 2.4. 224 pgs.

Gibbs J.F., D.M. Boore, W.B. Joyner and T.E. Fumal, 1994. The Attenuation of Seismic Shear Waves in Quaternary Alluvium in Santa Clara Valley, California. Bulletin of the Seismological Society of America, 84 (1), 76-90.

Government of Canada, 2013. Interdepartmental Letter of Agreement between Natural Resources Canada and Health Canada, Contract #4500295328, 14 pgs.

Griffin M.J., 1996. Handbook of Human Vibration, Elsevier Academic Press, London, United Kingdom. 998 pgs.

Justus C.G., W.R. Hargraves and A. Yalcin, 1976. Nationwide Assessment of Potential Output from Wind-Powered Generators, Journal of Applied Meteorology, 15 (7), 673-678.

Møller H. and C.S. Pedersen, 2011. Low-frequency noise from large wind turbines, Journal of the Acoustical Society of America, 129 (6), 3727-3744.

Nuta E., C. Christopoulos, and J.A. Packer, 2011. Methodology for seismic risk assessment for tubular steel wind turbine towers: application to Canadian seismic environment, Canadian Journal of Civil Engineering, 38, 293–304.

Nuttli O.W., 1973. Seismic Wave Attenuation and Magnitude Relations for Eastern North America, Journal of Geophysical Research, 78 (5), 876-885.

Panofsky H. and J. Dutton, 1984. Atmospheric Turbulence: models and methods for engineering applications. Pennsylvania State University: John Wiley and Sons, 1984.

Peterson J., 1993. Observation and modeling of seismic background noise, United States Geological Survey Technical Report, 93-322, 94 pgs.

Saccorotti G., D. Piccinini, L. Cauchie, and I. Fiori, 2011. Seismic Noise by Wind Farms: A Case Study from the Virgo Gravitational Wave Observatory, Italy, Bulletin of the Seismological Society of America, 101 (2), 568–578, doi: 10.1785/0120100203.

Schofield R., 2002. Seismic measurements at the Stateline Wind Project. Technical Report, LIGO-T020104-00-Z. 14 pgs.

Seguro J.V., and T.W. Lambert, 2000. Modern estimation of the parameters of the Weibull wind speed distribution for wind energy analysis, Journal of Wind Engineering and Industrial Aerodynamics, 85, 75–84.

Styles P., I. Stimpson, S. Toon, R. England and M. Wright, 2005. Microseismic and infrasound monitoring of low frequency noise and vibrations from windfarms. Recommendations of the siting of windfarms in the vicinity of Eskdalemuir, Scotland, Applied and Environmental Geophysics Technical Report, University of Keele. 125 pgs.

Styles P., 2010. An Assessment of the REACTEC/Wind Energy damping system for reduction of ground vibration in the 3 to 6 Hz band and the implications for Eskdalemuir IMS seismometer array station. Applied Environmental Geophysics Technical Report, University of Keele, 47 pgs.

van den Berg G.P., 2005. The Beat is Getting Stronger: The Effect of Atmospheric Stability on Low Frequency Modulated Sound of Wind Turbines, Journal of Low Frequency Noise, Vibration and Active Control, 24 (1), 1-24.

Vestas, 2006. General Specification: V90 – 3.0 MW VCRS 60 Hz, Item no. 950010.R5, 29 pgs.

Welch, P.D., 1967. The Use of Fast Fourier Transform for the Estimation of Power Spectra: A Method Based on Time Averaging Over Short, Modified Periodograms, IEEE Transactions on Audio Electroacoustics, AU-15, 70–73.

Wood, H.O., and F. Neumann, 1931. Modified Mercalli Intensity Scale of 1931, Bulletin of the Seismological Society of America, 21, 277-283.

Xi Engineering Consultants Ltd., 2014. Seismic vibration produced by wind turbines in the Eskdalemuir region, Research Report: FMB_203_FINAL_V5R, 98 pgs.